

# Meta Fusion: A Unified Framework For Multimodality Fusion with Mutual Learning

Ziyi Liang<sup>1</sup>, Annie Qu<sup>2</sup>, and Babak Shahbaba<sup>\*1</sup>

<sup>1</sup>Department of Statistics, University of California, Irvine, CA, USA

<sup>2</sup>Department of Statistics and Applied Probability, University of California, Santa Barbara, CA, USA

July 29, 2025

## Abstract

Developing effective multimodal data fusion strategies has become increasingly essential for improving the predictive power of statistical machine learning methods across a wide range of applications, from autonomous driving to medical diagnosis. Traditional fusion methods, including early, intermediate, and late fusion, integrate data at different stages, each offering distinct advantages and limitations. In this paper, we introduce **Meta Fusion**, a flexible and principled framework that unifies these existing strategies as special cases. Motivated by deep mutual learning and ensemble learning, Meta Fusion constructs a cohort of models based on various combinations of latent representations across modalities, and further boosts predictive performance through *soft information sharing* within the cohort. Our approach is model-agnostic in learning the latent representations, allowing it to flexibly adapt to the unique characteristics of each modality. Theoretically, our soft information sharing mechanism reduces the generalization error. Empirically, Meta Fusion consistently outperforms conventional fusion strategies in extensive simulation studies. We further validate our approach on real-world applications, including Alzheimer’s disease detection and neural decoding.

**Keywords:** Multimodality fusion; deep mutual learning; ensemble selection; representation learning; soft information sharing.

## 1 Introduction

Modern scientific research often involves processing and analyzing large amounts of data from diverse sources to extract information, make discoveries, and support decision-making. Effectively integrating these complex, multimodal data can lead to more holistic and rigorous solutions to scientific problems. For example, autonomous driving combines multiple

---

<sup>\*</sup>Corresponding author: [babaks@uci.edu](mailto:babaks@uci.edu)

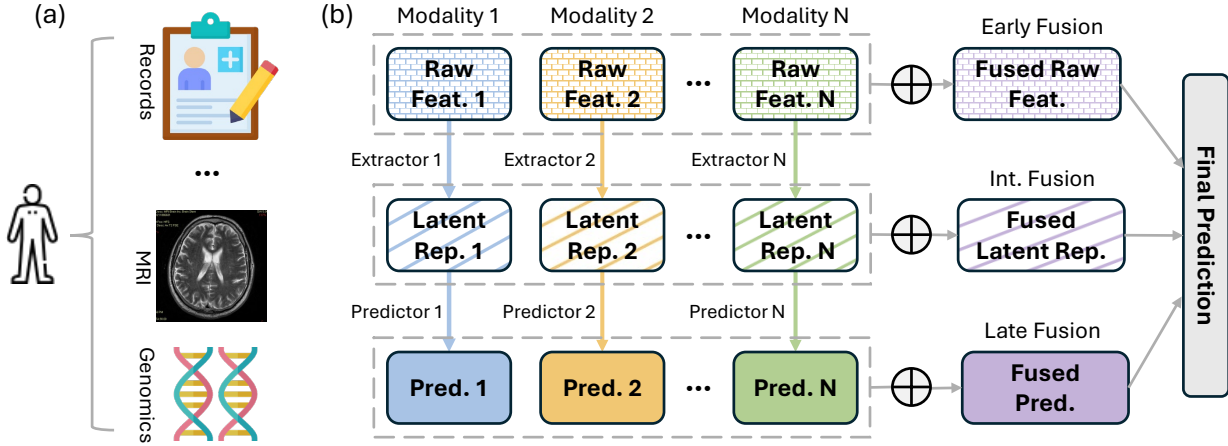


Figure 1: Overview of classical multimodal fusion strategies. (a) Example of multimodal data sources used in medical diagnosis, including patient records, MRI scans, and genomic data. (b) Illustration of the three broad fusion categories: early fusion, late fusion and intermediate fusion.

sensors for safe navigation [1, 2]. Sentiment analysis uses text, video, and audio to interpret emotions like humans do with multiple senses [3–5]. Medical diagnosis often integrates demographics, medical history, functional assessment, and imaging data [6, 7]. Consequently, developing effective multimodal data fusion strategies has become crucial to enhancing our understanding of scientific mechanisms and improving the predictive accuracy of statistical machine learning models.

## 1.1 Key questions: how to fuse, and what to fuse

Most existing research in multimodality fusion centers around two pivotal questions: how to fuse and what to fuse. The first addresses the encompassing fusion structure, while the second focuses on representation learning of multimodal data.

**How to fuse?** Existing data fusion frameworks can be broadly categorized into early, late, and intermediate fusion (Figure 1), based on the stage at which fusion occurs [8, 9]. Therefore, this question can also be framed as: “When to fuse?” *Early fusion* [10, 11] combines raw modalities before feature extraction, retaining all pertinent information and capturing rich cross-modal interactions. However, it is prone to overfitting in high-dimensional feature spaces and may perform poorly with highly heterogeneous and noisy modalities. *Late fusion* [12–14], or decision-level fusion, applies separate models to each modality and then aggregates their predictions. This approach is simple, robust, but suboptimal when the prediction task strongly depends on interactions or complementary information across modalities [8, 15]. *Intermediate fusion* [16–18] finds a common ground by fusing latent representations extracted from each modality, but its effectiveness largely depends on the quality of the learned latent representations.

**What to fuse?** A crucial step in data fusion is feature extraction, which involves learning low-dimensional latent representations to reduce noise and capture essential information from raw data. Early fusion seeks to learn a joint latent representation for all modalities simultaneously, as in multimodal Deep Boltzmann Machines [19] or multimodal encoder-based methods [20, 21]. Intermediate fusion typically employs separate unimodal feature extractors. However, a key challenge lies in selecting appropriate latent dimensions for each modality since mis-specifying these dimensions can severely hinder the overall performance of the fusion process.

## 1.2 Main contribution

Although many solutions have been proposed for specific applications [11, 16, 17], comprehensive and reliable answers to these central questions remain elusive. In this work, we aim to address this gap by proposing a data-driven framework, called *Meta Fusion*, that automatically determines when to fuse and what to fuse. Our approach starts with constructing a cohort of heterogeneous models, each focusing on different combinations of latent representations across modalities. These models are trained using a novel soft information sharing mechanism inspired by deep mutual learning [22]. Rather than learning their assigned tasks independently, models in our framework are encouraged to align their outputs with those of the top performers in the cohort. Importantly, only outputs, rather than model parameters or latent representations, are shared during updates. This preserves cohort diversity, a reason we name it “soft information sharing.” Finally, we form a decision-making committee among the cohort through ensemble learning techniques [23, 24] and aggregate the committee’s predictions.

Our key contributions include: First, we develop a task-agnostic and model-agnostic framework that provides a unified solution for multimodal fusion problems. Most existing benchmarks, as shown in Section 3.2, can be viewed as special cases of this unifying framework. Second, we introduce a soft information sharing strategy through adaptive mutual learning that dynamically determines which information to share within the cohort. Specifically, we screen for top performers in the cohort and let others learn from them but not vice versa to avoid negative knowledge transfer. Our theoretical analysis shows that this strategy reduces individual model generalization error under appropriate conditions. To our knowledge, this is the first theoretical analysis of deep mutual learning and may be of independent interest in a broad context as it offers insights into the optimization landscape. Third, we demonstrate *Meta Fusion*’s effectiveness through extensive numerical studies and applications to early detection of Alzheimer’s disease and decoding of neuronal activities in the hippocampus.

## 1.3 Organization

The paper is organized as follows. Section 2 reviews related work. Section 3 presents *Meta Fusion*, with methodological details in Section 3.1 and connections to existing benchmarks in Section 3.2 (with additional details in Appendix A2). Section 4 provides the theoretical results. Section 5 and Section 6 present simulation experiments and real-world data analysis, respectively. Section 7 concludes with a discussion and suggestions for future directions. Im-

plementation details and additional numerical experiments are provided in Appendix A1 and Appendix A3 respectively. Appendix A4 contains all mathematical proofs and Appendix A5 includes supplementary tables and figures.

## 2 Related work

### 2.1 Cooperative learning for multiview analysis

Among recent fusion strategies, the cooperative learning approach proposed by Ding et al. [15] is particularly relevant to our work, as it also aims to develop a framework that automatically determines when to fuse. Consider two modalities as random variables  $X \in \mathbb{R}^{p_x}$  and  $Z \in \mathbb{R}^{p_z}$  with ground truth label  $Y \in \mathbb{R}$ , where  $p_x, p_z \in \mathbb{Z}$  are feature dimensions. Cooperative learning minimizes the following population quantity for a given hyperparameter  $\rho \in [0, 1]$ :

$$\begin{aligned} \min_{f_X, f_Z, f_{XZ}} \mathbb{E} \left\{ \frac{1}{2} (Y - f_X(X) - f_Z(Z) - f_{XZ}(X, Z))^2 \right. \\ \left. + \frac{\rho}{2} (f_X(X) - f_Z(Z))^2 + \frac{\rho}{2(1-\rho)} f_{XZ}^2(X, Z) \right\}. \end{aligned} \quad (1)$$

The expectation is taken over the randomness of  $X$  and  $Z$ . Here,  $f_X$ ,  $f_Z$  are unimodal predictors, and  $f_{XZ}$  is a joint predictor capturing feature interactions. The first term in (1) is the mean squared error; the second is a penalty encouraging agreement between modalities; and the third controls the contribution of the interaction term. Ding et al. [15] show that (1) admits fixed points:

$$\begin{aligned} f_X(X) &= \mathbb{E} \left\{ \frac{Y}{1+\rho} - \frac{(1-\rho)f_Z(Z)}{(1+\rho)} - \frac{f_{XZ}(X, Z)}{1+\rho} \mid X \right\}, \\ f_Z(Z) &= \mathbb{E} \left\{ \frac{Y}{1+\rho} - \frac{(1-\rho)f_X(X)}{(1+\rho)} - \frac{f_{XZ}(X, Z)}{1+\rho} \mid Z \right\}, \\ f_{XZ}(X, Z) &= \mathbb{E} \left\{ (1-\rho)(Y - f_X(X) - f_Z(Z)) \mid X, Z \right\}. \end{aligned} \quad (2)$$

By adjusting  $\rho$ , cooperative learning can interpolate between early and late fusion. When  $\rho = 0$ , (1) reduces to the additive model  $f_X(X) + f_Z(Z) + f_{XZ}(X, Z)$ , equivalent to early fusion if the functions are additive. As  $\rho \rightarrow 1$ , it is clear from (2) that the joint function  $f_{XZ}$  vanishes, and the solution converges to  $0.5\mathbb{E}(Y \mid X) + 0.5\mathbb{E}(Y \mid Z)$ , corresponding to late fusion via averaging the marginal predictions. In practice,  $\rho$  is selected through cross-validation, offering a data-driven way to determine when to fuse modalities. However, cooperative learning has limitations. First, it does not fully address what to fuse: the joint function  $f_{XZ}$  is trained on the combined features of both modalities, which can lead to poor performance in high-dimensional or heterogeneous settings. While Ding et al. [15] recommend using Lasso [25] for feature selection in linear settings, it remains unclear how to effectively reduce dimensionality for complex models in nonlinear contexts. This issue also affects the unimodal predictors. Since the final prediction is the sum of  $f_X$ ,  $f_Z$ , and  $f_{XZ}$ , overfitting in any component may degrade overall performance. Second, the framework is tailored to regression tasks using mean squared error, and its adaptation to classification remains an open problem.

## 2.2 Deep mutual learning

Deep mutual learning extends knowledge distillation [26, 27] to a cohort of *student* models that learn collaboratively by sharing information with one another. In addition to optimizing their task-specific losses, these models also align their outputs during training. The original mutual learning framework [22] is designed for single-modal data and homogeneous students, where models with identical architectures are trained in parallel with different initializations. More recently, deep mutual learning has been extended to multimodal fusion [28–31], typically assigning one model per modality and applying standard mutual learning, which treats all students equally. This approach might be suboptimal in the presence of noisy or heterogeneous modalities, as demonstrated by our theoretical and experimental findings (Section 4 and Appendix A3.2). In contrast, Meta Fusion introduces adaptive mutual learning to selectively determine which models to learn from and effectively mitigate negative knowledge transfer.

## 3 Methodology

### 3.1 Meta Fusion

To address the above issues, we propose Meta Fusion, a novel mutual learning framework for multimodal data fusion that flexibly extracts and integrates information from diverse data sources. As illustrated in Figure 2, Meta Fusion consists of *three main steps*. First, we construct a cohort of student models (Section 3.1.1), each receiving different combinations of latent representations from the available modalities. These student models may have varying architectures to accommodate the heterogeneity of the input data. Second, as described in Section 3.1.2, the cohort undergoes adaptive mutual learning to facilitate soft information sharing. We use a data-driven approach to identify the top-performing student models and allow the others to learn from them, thereby reducing the risk of negative knowledge transfer. This approach contrasts with conventional mutual learning [22], which treats all student models equally. Finally, we aggregate the predictions of the cohort using ensemble techniques, such as ensemble selection (Section 3.1.3), to produce the final output.

#### 3.1.1 Constructing the student cohort

Rather than relying on a single model to capture and integrate information from all modalities, we construct a set of models called “students”. We refer to their collection as a “student cohort” [22]. Each student can have a different structure or focus on different modalities to promote diversity of feature learning. Given samples from two modalities,  $\mathbf{X} \in \mathbb{R}^{n \times p_x}$ ,  $\mathbf{Z} \in \mathbb{R}^{n \times p_z}$ , where  $n \in \mathbb{Z}$  is the sample size, we use  $k_x > 1$  feature extractors for  $\mathbf{X}$ , denoted as  $g_x^i(\mathbf{X})$  for  $i \in [k_x]$ , and  $k_z > 1$  extractors for  $\mathbf{Z}$ , denoted as  $g_z^j(\mathbf{Z})$  for  $j \in [k_z]$ . Extractors are tailored to each modality. For example, convolutional networks or pre-trained models like ResNet [32] for images, and BERT [33] for text. Different extractors, or outputs from various layers, yield diverse latent representations, capturing information at multiple resolution levels. We also introduce two dummy extractors for each modality: an identity mapping,  $g_x^{k_x+1}(\mathbf{X}) := \mathbf{X}$  and  $g_z^{k_z+1}(\mathbf{Z}) := \mathbf{Z}$ , which preserves all raw features, and a null

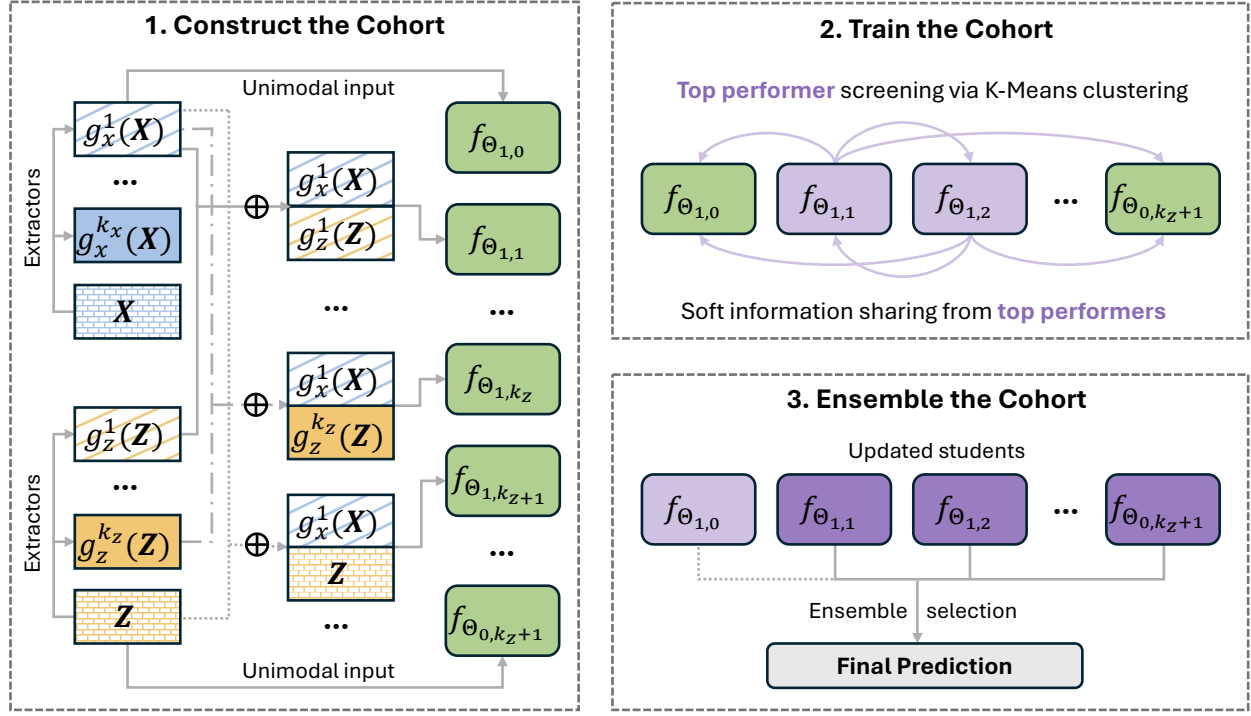


Figure 2: Overview of the Meta Fusion pipeline.

mapping,  $g_x^0(\mathbf{X}) := \emptyset$  and  $g_x^0(\mathbf{Z}) := \emptyset$ , which excludes the corresponding modality.

Given the extractors  $\{g_x^i(\mathbf{X})\}_{i \in \{0, \dots, k_x+1\}}$  and  $\{g_z^j(\mathbf{Z})\}_{j \in \{0, \dots, k_z+1\}}$ , we fuse their outputs to construct student models by using a cross-modality pairing strategy, illustrated in the left panel of Figure 2. That is, each latent representation of  $\mathbf{X}$ ,  $g_x^i(\mathbf{X})$  for  $i \in \{0, 1, \dots, k_x+1\}$ , is paired with a latent representation of  $\mathbf{Z}$ ,  $g_z^j(\mathbf{Z})$  for  $j \in \{0, 1, \dots, k_z+1\}$  to form a student model. Pairings are combined as  $g_x^i(\mathbf{X}) \oplus g_z^j(\mathbf{Z})$ , where  $\oplus$  denotes column-wise concatenation. We exclude the null combination  $g_x^0(\mathbf{X}) \oplus g_z^0(\mathbf{Z})$ , and define the set of valid pairings as  $\mathcal{P} := \{\{0, \dots, k_x+1\} \times \{0, \dots, k_z+1\}\} \setminus \{(0, 0)\}$ . For each  $(i, j) \in \mathcal{P}$ , the fused representation is used as the input to train a supervised model:

$$f_{\Theta_{i,j}}(\mathbf{X}, \mathbf{Z}) := f_{i,j}(g_x^i(\mathbf{X}) \oplus g_z^j(\mathbf{Z})), \quad (3)$$

where  $f_{i,j}$  is the task-specific model, possibly varying in structures, and  $\Theta_{i,j}$  denotes trainable parameters. This yields a cohort of  $(k_x+2)(k_z+2) - 1$  students:  $k_x+1$  models use only  $\mathbf{X}$  (i.e.,  $f_{\Theta_{i,0}}$  for  $i \in [k_x+1]$ ),  $k_z+1$  use only  $\mathbf{Z}$  (i.e.,  $f_{\Theta_{0,j}}$  for  $j \in [k_z+1]$ ), and  $(k_x+1)(k_z+1)$  use both modalities, with  $f_{\Theta_{k_x+1,k_z+1}}$  retrieving the early fusion model that operates on concatenation of raw modalities. In practice, cohort size is flexible and can be adjusted for computational efficiency. This comprehensive pairing facilitates data-driven selection of optimal latent combinations.

### 3.1.2 Training the student cohort

Although model diversity can improve ensemble performance, recent studies have shown that optimal results depend on balancing diversity and predictive performance [34, 35];

maximizing diversity alone is not always ideal. In multimodal fusion, cross-modality pairing naturally increases diversity, but not all latent representations are equally beneficial for downstream tasks. To this end, we introduce a mutual learning framework that adaptively selects top-performing students and enables the cohort to learn from them, enhancing overall predictive performance through merit-guided information sharing across diverse ensemble representations.

Let  $\mathbf{Y} \in \mathbb{R}^n$  denote the ground-truth labels and  $\widehat{\mathbf{Y}}_I = f_{\Theta_I}(\mathbf{X}, \mathbf{Z}) \in \mathbb{R}^{n \times d}$  denote the prediction from student model  $f_{\Theta_I}$ , where  $d$  is the output dimension and  $I \in \mathcal{P}$  indexes a specific cross-modal pairing of latent features. Each student's loss consists of two components: a task-specific prediction loss,  $\mathcal{L}(\widehat{\mathbf{Y}}_I, \mathbf{Y})$ , and a divergence loss that encourages agreement with other cohort members:

$$\mathcal{L}_{\Theta_I} = \underbrace{\mathcal{L}(\widehat{\mathbf{Y}}_I, \mathbf{Y})}_{\text{task loss}} + \rho \underbrace{\sum_{J \in \mathcal{P}, J \neq I} d_{I,J} \mathcal{D}(\widehat{\mathbf{Y}}_I, \widehat{\mathbf{Y}}_J)}_{\text{divergence loss}}, \quad (4)$$

where  $\mathcal{D}(\widehat{\mathbf{Y}}_I, \widehat{\mathbf{Y}}_J)$  measures the divergence between students  $I$  and  $J$ . The objective in (4) is task-agnostic: for regression, Mean Squared Error (MSE) can be used for both the task and divergence terms, while for classification, Cross-Entropy Loss is suitable for the task loss and Kullback-Leibler (KL) divergence for the second term.

The hyperparameter  $\rho > 0$ , determined via cross-validation, controls the balance between the two loss terms. The weights  $d_{I,J} \geq 0$  determine the influence of each peer in the divergence loss. In standard mutual learning,  $\rho = 1$  and  $d_{I,J} = 1$  for all  $I, J \in \mathcal{P}, J \neq I$ , so each student learns from all others—an approach that is more suitable for homogeneous, single-modal data. However, in the multimodal case, students may be highly heterogeneous due to differing modality combinations or architectures, resulting in varying performance across the cohort. If student  $I$  performs significantly worse than others, it can be advantageous to set its associated  $d_{J,I}$  for  $J \in \mathcal{P}, J \neq I$  to zero or a small value to avoid negative knowledge transfer. To address this, we propose a two-step adaptive mutual learning procedure: first, determine the divergence weights  $d_{I,J}$  in a data-driven way, then train the cohort using these optimized weights.

### Step 1: Initial Screening

To determine appropriate weights  $\{d_{I,J}\}_{I,J \in \mathcal{P}, I \neq J}$  and prevent negative learning, models are first trained independently using only the task loss, namely,  $\rho = 0$  in (4). After this phase, each student's initial loss,  $\{L_{\Theta_I}^{\text{init}}\}_{I \in \mathcal{P}}$  is evaluated on a holdout validation set  $\mathcal{D}^{\text{val}} \subset \{\mathbf{X}, \mathbf{Z}, \mathbf{Y}\}$ . Next, we apply K-Means clustering to the set of initial losses  $\{L_{\Theta_I}^{\text{init}}\}_{I \in \mathcal{P}}$  to group students into  $k_{\text{cls}} > 1$  performance-based clusters. The value of  $k_{\text{cls}}$  can be chosen automatically using approaches such as the Silhouette method [36] or the Elbow method [37]. Let  $\mathcal{S} = \{S_1, \dots, S_{k_{\text{cls}}}\}$ , where  $\cup_{k \in [k_{\text{cls}}]} S_k = \mathcal{P}$ , denote the resulting partition of the model indices  $\mathcal{P}$ .

We define  $\mathcal{S}_{\text{top}}$  as the set of models belonging to the best-performing  $k_{\text{top}} \geq 1$  clusters with the lowest average initial loss. The divergence weights are then set according to cluster

---

**Algorithm 1** Training with Adaptive Mutual Learning

---

- 1: **Input:** Student models  $f_{\Theta_I}$  for  $I \in \mathcal{P}$ ; multimodal dataset  $(\mathbf{X}, \mathbf{Z})$ ; label set  $\mathbf{Y}$ ; epochs  $n_t$ ; and mutual learning parameter  $\rho^* > 0$ .
- 2: Randomly initialize student parameters  $\Theta_I$  for all  $I \in \mathcal{P}$ .
- 3: Randomly split the multimodal data into two disjoint subsets  $\mathcal{D}^{\text{train}}$  and  $\mathcal{D}^{\text{val}}$ .
- 4: **Step 1: Initial Screening**
  - 5: Train  $\Theta_I$  for all  $I \in \mathcal{P}$  for  $n_t$  epochs by minimizing the loss in (4) with  $\rho = 0$ .
  - 6: Evaluate the initial task loss  $\{L_{\Theta_I}^{\text{init}}\}_{I \in \mathcal{P}}$  on the holdout data  $\mathcal{D}^{\text{val}}$ .
  - 7: Compute the divergence weights  $\{d_{I,J}\}_{I,J \in \mathcal{P}, I \neq J}$  with Equation (5).
- 8: **Step 2: Mutual Learning**
  - 9: Re-initialize student parameters  $\Theta_I$  for all  $I \in \mathcal{P}$ .
  - 10: Train  $\Theta_I$  for all  $I \in \mathcal{P}$  for  $n_t$  epochs by minimizing the loss in (4) with  $\rho = \rho^*$  and  $\{d_{I,J}\}_{I,J \in \mathcal{P}, I \neq J}$  obtained in **Step 1**.
- 11: **Output:** Updated student cohort  $f_{\Theta_I}$  for  $I \in \mathcal{P}$ .

---

membership:

$$d_{I,J} = \begin{cases} 1, & \text{if } J \in \mathcal{S}_{\text{top}} \\ 0, & \text{otherwise.} \end{cases} \quad (5)$$

That is, model  $I$  learns from model  $J$  only if  $J$  is identified as a top performer in the initial screening. This strategy prioritizes students with stronger initial performance, potentially due to superior architectures or informative cross-modal features. By adaptively setting the divergence weights, we enable weaker models to benefit from the best performers, while protecting top students from negative influence during mutual learning.

### Step 2: Soft Information Sharing via Adaptive Mutual Learning

With the divergence weights  $\{d_{I,J}\}_{I,J \in \mathcal{P}, I \neq J}$  determined and a fixed hyperparameter  $\rho > 0$  (selected via cross-validation), the student cohort is jointly trained for  $n_t > 0$  epochs by minimizing the overall loss in (4) using gradient descent. Training can be performed in parallel for efficiency. With  $\rho > 0$ , student models are guided to align with top-performing peers during each update, promoting learning through soft information sharing. This process preserves diversity (since model parameters are not exchanged directly) while encouraging consensus by aligning model outputs, thus improving predictive performance and maintaining beneficial differences among students. Overall, this mutual learning step helps balance the trade-off between diversity and predictive performance [34]. We further demonstrate theoretically in Section 4 that, under suitable conditions, this adaptive mutual learning strategy effectively reduces the generalization error of individual students. The two step training procedure of the student cohort is summarized in Algorithm 1.

#### 3.1.3 Aggregating the student cohort

After training the student cohort, we aggregate their predictions using ensemble techniques to obtain a final, unified prediction. Any standard ensemble method appropriate for the

---

**Algorithm 2** Forming Decision-making Committee with Ensemble Selection

---

```
1: Input: Student models  $f_{\Theta_I}$  for  $I \in \mathcal{P}$ ; validation set  $\mathcal{D}^{\text{val}}$ ; pruning proportion  $p_{\text{prune}}$ ; number of initial models  $n_{\text{init}} > 0$ ; maximum committee size  $n_c > 0$ ; ensemble loss function  $\mathcal{L}^{\text{ens}}(\mathcal{C}, \mathcal{D})$  for committee  $\mathcal{C}$  on data  $\mathcal{D}$ .
2: Evaluate and sort the task-specific loss of each  $f_{\Theta_I}$  for  $I \in \mathcal{P}$  using  $\mathcal{D}^{\text{val}}$ .
3: Prune the lowest-performing  $p_{\text{prune}}$  fraction of students.
4: Initialize the committee  $\mathcal{C}$  with  $n_{\text{init}}$  best-performing students.
5: Set  $\mathcal{P}_{\text{avail}} \subset \mathcal{P}$  to all remaining students after pruning and initialization.
6: while  $|\mathcal{C}| < n_c$  do
7:   For each  $I \in \mathcal{P}_{\text{avail}}$ , evaluate  $\mathcal{L}^{\text{ens}}(\mathcal{C} \cup \{I\}, \mathcal{D}^{\text{val}})$ .
8:   Select  $I^* = \arg \min_{I \in \mathcal{P}_{\text{avail}}} \mathcal{L}^{\text{ens}}(\mathcal{C} \cup \{I\}, \mathcal{D}^{\text{val}})$ .
9:   if  $\mathcal{L}^{\text{ens}}(\mathcal{C} \cup \{I^*\}, \mathcal{D}^{\text{val}}) < \mathcal{L}^{\text{ens}}(\mathcal{C}, \mathcal{D}^{\text{val}})$  then
10:    Add  $I^*$  to committee:  $\mathcal{C} \leftarrow \mathcal{C} \cup \{I^*\}$ .
11:    Remove  $I^*$  from  $\mathcal{P}_{\text{avail}}$ :  $\mathcal{P}_{\text{avail}} \leftarrow \mathcal{P}_{\text{avail}} \setminus \{I^*\}$ .
12:   else
13:     break
14:   end if
15: end while
16: Output: The decision-making committee  $\mathcal{C}$ .
```

---

task may be used, e.g., stacking, or averaging (see Appendix A1.3 for an overview). Given the heterogeneous nature of the cohort, we adopt *ensemble selection* [24, 38] to form a robust decision-making committee  $\mathcal{C} \subseteq \mathcal{P}$ . This method builds the ensemble by iteratively adding models that improve validation performance, optimizing for a chosen metric. To enhance efficiency and robustness, we first rank the models by task-specific loss on a holdout set  $\mathcal{D}^{\text{val}}$ , and prune the lowest-performing  $p_{\text{prune}} \in (0, 1)$  fraction. We initialize  $\mathcal{C}$  with  $n_{\text{init}} > 0$  top performers, then iteratively add models from the remaining candidates that yield the greatest improvement in ensemble performance, which may be evaluated via simple or weighted averaging. The detailed procedure is outlined in Algorithm 2.

Ensemble selection maximizes performance by forming a robust committee using the most effective models, avoiding the inclusion of weaker models that could reduce overall quality. While both initial K-Means screening (Algorithm 1) and ensemble selection (Algorithm 2) identify strong performers, the former quickly filters students for mutual learning robustness, while the latter optimizes the final committee for ensemble performance. Notably, students who do not excel initially may improve and be selected for the final ensemble.

### 3.2 Relation to existing methods

Many widely used methods can be viewed as special cases of our proposed unified approach, offering insight into the superior performance observed in our experiments (Sections 5 to 6). Classical paradigms of multimodal fusion, namely early, intermediate, and late fusion, are all encompassed within our unified framework. Specifically, our model reduces to early fusion when there is a single student,  $f_{\Theta_{k_x+1, k_z+1}}(\mathbf{X}, \mathbf{Z})$ , which operates on the concatenation of raw

modalities. Intermediate fusion is similarly recovered when only one student  $f_{\Theta_{i,j}}(\mathbf{X}, \mathbf{Z})$  with arbitrary feature extractors,  $g_x^i(\mathbf{X})$  and  $g_z^j(\mathbf{Z})$  for any  $i \in [k_x], j \in [k_z]$ , is considered. Late fusion fits within our framework as a cohort of two students  $f_{\Theta_{k_x+1,0}}(\mathbf{X}, \mathbf{Z})$ , operating only on  $\mathbf{X}$  and  $f_{\Theta_{0,k_z+1}}(\mathbf{X}, \mathbf{Z})$  operating only on  $\mathbf{Z}$ , where both models are trained independently without mutual learning.

Cooperative learning can also be viewed as a special case, albeit in a more nuanced way. Appendix A2 analyzes a simplified form of the cooperative learning objective in (1) that excludes explicit cross-modal interactions. The simplified objective is the primary focus in Ding et al. [15] and Appendix A2 shows that it is equivalent to Meta Fusion using two single-modality students aggregated with simple averaging.

Finally, several existing multimodal fusion methods employing deep mutual learning techniques [28–31] can also be seen as special cases of our approach. In these cases, unimodal students are trained using non-adaptive mutual learning, with parameters  $\rho = 1$  and  $d_{I,J} = 1$  for any student pair  $(I, J)$ . This approach does not facilitate interactions between cross-modal features, which may lead to poor performance when modalities provide complementary information. Additionally, non-adaptive mutual learning can lead to degraded performance in the presence of noisy or adversarial modalities.

### 3.3 Extension to multiple modalities

Our framework readily extends to settings with more than two modalities. The main consideration is constructing the cross-modal student cohort; the processes for cohort training via adaptive mutual learning (Section 3.1.2) and final prediction through ensemble selection (Section 3.1.3) remain unchanged. Appendix A1.1 describes how to generalize the cross-modal pairing strategy in Section 3.1.1 to build student cohorts for applications involving more than two modalities.

## 4 Theoretical properties

### 4.1 Notations

By convention, we use boldface to denote vectors or matrices (e.g.  $\mathbf{0}$  for vector of zeros and 0 for scalar.) Additionally, we define the following technical notations: For a matrix  $\mathbf{M}$ ,  $\mathbf{M}_{i:}$  denotes the  $i$ -th row and  $\mathbf{M}_{:i}$  denotes the  $i$ -th column. For matrices  $\mathbf{M}_I, \mathbf{M}_J$  indexed by  $I, J \in \mathcal{P}$ , we denote  $\mathbf{M}_I^\top \mathbf{M}_J$  as  $\mathbf{M}_{IJ}$  for simplicity. For  $\mathbf{x} \in \mathbb{R}^d$ ,  $\mathbf{x}^{\circ 2} := (x_1^2, \dots, x_d^2)$  denotes the element-wise square, and  $\text{Var}^\circ(\mathbf{x}) := (\text{Var}(x_1), \dots, \text{Var}(x_d))$  denotes the element-wise variance.

### 4.2 Main theories

In this section, we present the theoretical properties of the proposed Meta Fusion framework. Although Meta Fusion is both task-agnostic and model-agnostic by design, for clarity and tractability, we focus our theoretical analysis on regression tasks using mean squared error (MSE) as the loss function.

We assume the ground-truth labels  $\mathbf{Y} = (Y_1, \dots, Y_n) \in \mathbb{R}^n$  are generated from a latent factor model,  $\mathbf{Y} = \mathbf{V}\boldsymbol{\theta}$  for some coefficients  $\boldsymbol{\theta} \in \mathbb{R}^p$  and latent factors  $\mathbf{V} \in \mathbb{R}^{n \times p}$ . Assume  $\mathbf{V}_{i:}$  follows a multivariate Gaussian distribution, independently for each  $i \in [n]$  with

$$\mathbf{V}_{i:} \sim N(\mathbf{0}, \boldsymbol{\Sigma}), \quad (6)$$

where  $\boldsymbol{\Sigma} \in \mathbb{R}^{p \times p}$  is the identity matrix.

Consider the general case with  $M \geq 2$  modalities  $\mathbf{X}_m$ . For any student model  $I = (i_1, \dots, i_M) \in \mathcal{P}$ , denote the fused presentation as  $\mathbf{V}_I := \bigoplus_{m=1}^M g_m^{i_m}(\mathbf{X}_m)$ , where each  $g_m^{i_m}$  is a feature extractor for modality  $\mathbf{X}_m$  (see Appendix A1.1). In our theoretical analysis, we assume a signal-plus-noise model for the fused representations where each  $\mathbf{V}_I$  is modeled as a noisy transformation of the oracle latent factors  $\mathbf{V}$ .

**Assumption 1.** *For a student model  $I \in \mathcal{P}$ , the fused representation satisfies*

$$\mathbf{V}_I = \mathbf{V}\mathbf{T}_I + \boldsymbol{\epsilon}_I, \quad (7)$$

where  $p_I$  is the feature dimension of  $\mathbf{V}_I$  and  $\mathbf{T}_I \in \mathbb{R}^{p \times p_I}$  is a linear transformation,  $\boldsymbol{\epsilon}_{I:} \sim N(0, \sigma_I^2 \boldsymbol{\Sigma}_I)$  with  $\sigma_I > 0$ , and  $\boldsymbol{\Sigma}_I \in \mathbb{R}^{p_I \times p_I}$  is the identity matrix.

We assume the features of the fused latent representations are independent. This assumption is standard in the literature, as it enables analytical simplifications [39], and preprocessing steps such as PCA are often employed to promote feature independence.

**Assumption 2.** *For  $I \in \mathcal{P}$ , we assume  $\mathbf{T}_I \in \mathbb{R}^{p \times p_I}$  has orthogonal columns:  $\mathbf{T}_{I:i}^\top \mathbf{T}_{I:j} = 0$ .*

We analyze our method with a cohort of two students, i.e.,  $\mathcal{P} = \{I, J\}$  with  $d_{I,J} = 1$ . Each student's supervised model is a deep linear network, a neural network without activation functions. Although deep linear networks do not have greater capacity than simple linear regressors, they are frequently used as a foundation for understanding the behavior of deeper, nonlinear networks [40–43].

Let  $\boldsymbol{\theta}_I \in \mathbb{R}^{p_I}$  and  $\boldsymbol{\theta}_J \in \mathbb{R}^{p_J}$  be the model parameters for student  $I, J$ , respectively. One can show that optimizing the individual objectives in (4) is equivalent to minimizing the following combined loss, since both yield the same gradients:

$$\mathcal{L}_{(\boldsymbol{\theta}_I, \boldsymbol{\theta}_J)} = \|\mathbf{Y} - \mathbf{V}_I \boldsymbol{\theta}_I\|^2 + \|\mathbf{Y} - \mathbf{V}_J \boldsymbol{\theta}_J\|^2 + \rho \|\mathbf{V}_I \boldsymbol{\theta}_I - \mathbf{V}_J \boldsymbol{\theta}_J\|^2. \quad (8)$$

The parameters are estimated by minimizing the empirical objective above, namely,

$$(\hat{\boldsymbol{\theta}}_I, \hat{\boldsymbol{\theta}}_J) = \underset{\boldsymbol{\theta}_I \in \mathbb{R}^{p_I}, \boldsymbol{\theta}_J \in \mathbb{R}^{p_J}}{\operatorname{argmin}} \mathcal{L}_{(\boldsymbol{\theta}_I, \boldsymbol{\theta}_J)}. \quad (9)$$

Our first theoretical result shows that the global minimizer  $\hat{\boldsymbol{\theta}}_I$  depends on the disagreement penalty  $\rho$ . Notably,  $\hat{\boldsymbol{\theta}}_I$  is also a function of  $\mathbf{V}_J$ , indicating that student  $J$  effectively shares information with  $I$  through mutual learning, without directly disclosing its latent representations. Since students  $I$  and  $J$  play symmetric roles, all subsequent analysis for  $I$  applies equally to  $J$  by swapping indices.

**Proposition 1.** Assume both students in  $\mathcal{P}$  satisfy Assumption 1, and  $n \geq \max\{p_I, p_J\}$ . The global minimizer  $\hat{\boldsymbol{\theta}}_I$  of the objective function in (8) takes the form of:

$$\hat{\boldsymbol{\theta}}_I = (1 - \rho) \mathbf{V}_{II}^{-1} \mathbf{V}_I^\top \mathbf{Y} + \rho \mathbf{V}_{II}^{-1} \mathbf{V}_{IJ} \mathbf{V}_{JJ}^{-1} \mathbf{V}_J^\top \mathbf{Y} + \mathbf{H}(\rho),$$

where  $\mathbf{H}(\rho) = \sum_{n=2}^{\infty} \rho^n \mathbf{G}_n$ , for some  $\mathbf{G}_n \in \mathbb{R}^{p_I}$  independent of  $\rho$ .

Next, we investigate how the choice of  $\rho$  influences the generalization error on an unseen *test point*. Let  $\mathbf{V}_* \in \mathbb{R}^p$  denote the oracle latent vector for the test point, independently drawn according to (6), and let  $Y_* = \mathbf{V}_*^\top \boldsymbol{\theta}$  be the ground-truth label. The fused representations for this test point,  $\mathbf{V}_{I*}, \mathbf{V}_{J*}$ , are defined as in (7). The generalization error for student  $I$  is given by:

$$\text{MSE}(I; \rho) = \mathbb{E} \left\{ (Y_* - \mathbf{V}_{I*}^\top \hat{\boldsymbol{\theta}}_I)^2 \mid \mathbf{V}_I \right\}. \quad (10)$$

We introduce several key quantities that will later allow us to decompose the generalization error for a clearer understanding. Let  $\tilde{\boldsymbol{\Sigma}}_I := \mathbf{T}_{II} + \sigma_I^2 \boldsymbol{\Sigma}_I$  and  $\boldsymbol{\theta}_I^* = \tilde{\boldsymbol{\Sigma}}_I^{-1} \mathbf{T}_I^\top \boldsymbol{\theta}$  be some oracle quantities defined with more details in Lemma A2 in the Appendix. For  $\mathbf{x} \in \mathbb{R}^d$ ,  $\mathbf{x}^{\circ 2}$  is the element-wise square, and  $\text{Var}^\circ(\mathbf{x})$  is the element-wise variance as defined in Section 4.1. With these, we define the following components:

$$\begin{aligned} B^2(\mathbf{V}_I; \rho) &= \text{diag} \left( \tilde{\boldsymbol{\Sigma}}_I \right)^\top \left\{ \mathbb{E}(\boldsymbol{\theta}_I^* - \hat{\boldsymbol{\theta}}_I \mid \mathbf{V}_I) \right\}^{\circ 2} \\ V_a(\mathbf{V}_I; \rho) &= \text{diag} \left( \tilde{\boldsymbol{\Sigma}}_I \right)^\top \mathbb{E} \left\{ \text{Var}^\circ(\hat{\boldsymbol{\theta}}_I \mid \mathbf{V}_I, \mathbf{V}_J) \mid \mathbf{V}_I \right\} \\ V_e(\mathbf{V}_I; \rho) &= \text{diag} \left( \tilde{\boldsymbol{\Sigma}}_I \right)^\top \text{Var}^\circ \left\{ \mathbb{E}(\hat{\boldsymbol{\theta}}_I \mid \mathbf{V}_I, \mathbf{V}_J) \mid \mathbf{V}_I \right\}, \end{aligned}$$

where  $B^2(\mathbf{V}_I; \rho)$  is the bias related term;  $V_a(\mathbf{V}_I; \rho)$  represents the **aleatoric** (intrinsic) variance, and  $V_e(\mathbf{V}_I; \rho)$  corresponds to the **epistemic** (knowledge-based) variance.

The first main theoretical result demonstrates that increasing the disagreement penalty  $\rho$  can reduce the generalization error, primarily by decreasing the intrinsic variance.

**Theorem 1.** Suppose both students in  $\mathcal{P}$  satisfy Assumption 1. Under Assumption 2, the generalization error given  $\mathbf{V}_I$  can be decomposed as follows:

$$\text{MSE}_I(\mathbf{V}_I; \rho) = \mathbb{E} \left\{ (Y_* - \mathbf{V}_{I*}^\top \hat{\boldsymbol{\theta}}_I)^2 \mid \mathbf{V}_I \right\} = B^2(\mathbf{V}_I; \rho) + V_a(\mathbf{V}_I; \rho) + V_e(\mathbf{V}_I; \rho) + \sigma_I^{*2},$$

with oracle quantity  $\sigma_I^{*2}$  defined in Lemma A2. Furthermore,

$$\frac{d}{d\rho} B^2(\mathbf{V}_I; \rho) \mid_{\rho=0} = 0, \quad \frac{d}{d\rho} V_e(\mathbf{V}_I; \rho) \mid_{\rho=0} = 0 + \mathcal{O}_p(n^{-1/2}), \quad \frac{d}{d\rho} V_a(\mathbf{V}_I; \rho) \mid_{\rho=0} = \Xi + \mathcal{O}_p(n^{-3/2})$$

where

$$\Xi = \frac{2\bar{\sigma}^{*2}}{n} \sum_{m=1}^{p_I} \left( \sum_{k=1}^{p_J} \frac{(\mathbf{T}_{J:k}^\top \mathbf{T}_{I:m})^2}{(\mathbf{T}_{I:m}^\top \mathbf{T}_{I:m} + \sigma_I^2)(\mathbf{T}_{J:k}^\top \mathbf{T}_{J:k} + \sigma_J^2)} - 1 \right) < 0,$$

and  $\bar{\sigma}^{*2} > 0$  is a constant defined in Lemma A1.

Equivalently, when both students receive informative latent representations satisfying Assumption 1, an increase in the disagreement penalty  $\rho$  does not effect the bias and the epistemic variance, but effectively reduce the aleatoric variance which in turn decreases the generalization error to the unobserved data.

Note that the generalization error in Theorem 1 is averaged over the randomness of  $\mathbf{V}_J$ . The next theorem examines the generalization error under specific realizations of  $\mathbf{V}_J$ , which reveals additional insight on how it changes with respect to both  $\mathbf{V}_I$  and  $\mathbf{V}_J$ .

**Theorem 2.** *Following the same conditions as in Theorem 1, let  $\mathbf{v}_I$  and  $\mathbf{v}_J$  be the realizations of  $\mathbf{V}_I$  and  $\mathbf{V}_J$ , respectively, and define the event*

$$\mathcal{E} = \left\{ \mathbf{v}_I, \mathbf{v}_J \mid \left( \mathbf{v}_{II}^{-1} \mathbf{v}_{IJ} \bar{\boldsymbol{\theta}}_J^* - (\boldsymbol{\theta}_I^* - \bar{\boldsymbol{\theta}}_I^*) \right) \succeq \mathbf{0} \text{ and } \left( \mathbf{v}_{II}^{-1} \mathbf{v}_{IJ} \mathbf{v}_{JJ}^{-1} \mathbf{v}_{JI} \bar{\boldsymbol{\theta}}_I^* - \bar{\boldsymbol{\theta}}_I^* \right) \preceq \mathbf{0} \right\},$$

where the notation  $\mathbf{x} \succeq \mathbf{y}$  (respectively,  $\mathbf{x} \preceq \mathbf{y}$ ) means for  $\mathbf{x}, \mathbf{y} \in \mathbb{R}^d$ ,  $x_i \geq y_i$  (respectively,  $x_i \leq y_i$ ) for all  $i \in [d]$ . Under event  $\mathcal{E}$ ,

$$\frac{d}{d\rho} B^2(\mathbf{V}_I; \rho) \mid_{\rho=0} \leq 0, \text{ and } \frac{d}{d\rho} V_e(\mathbf{V}_I; \rho) \mid_{\rho=0} \leq 0.$$

Conceptually, event  $\mathcal{E}$  requires that the latent representations of both students provide mutually supportive knowledge. Theorem 2 asserts that in such cases, Meta Fusion enhances each student's performance by reducing both bias and aleatoric variance.

The event  $\mathcal{E}$  introduced here is abstract. To provide more concrete intuition, the following corollary analyzes a simplified, low-dimensional case.

**Corollary 1.** *Under the same condition as in Theorem 2, consider the special case when  $p = p_I = p_J = 1$ . Then, the event  $\mathcal{E}$  in Theorem 2 simplifies to*

$$\mathcal{E} = \left\{ \mathbf{v}_I, \mathbf{v}_J \mid \frac{\mathbf{v}_I^\top \mathbf{v}_J}{\mathbf{v}_I^\top \mathbf{v}_I} \geq \frac{T_I T_J}{T_I^2 + \sigma_I^2} \right\}.$$

In this special case,  $\mathbf{v}_I, \mathbf{v}_J \in \mathbb{R}^n$  reduce to vectors, and  $T_I, T_J$  become scalars. Intuitively, this condition requires that the angle between  $\mathbf{v}_I$  and  $\mathbf{v}_J$  is not too large, ensuring that the latent representations from both students do not provide contradictory information.

## 5 Synthetic experiments

Using synthetic experiments to illustrate the effectiveness of the proposed method and compare its performance with existing methods. We use a latent factor model where the ground-truth label depends on four components: information specific to modality  $\mathbf{X}$ , information specific to modality  $\mathbf{Z}$ , shared information, and interaction terms between modalities. More specifically,

$$\mathbf{Y} = c_x \boldsymbol{\beta}_x f_x(\mathbf{X}^*) + c_z \boldsymbol{\beta}_z f_z(\mathbf{Z}^*) + c_s \boldsymbol{\beta}_s f_s(\mathbf{S}^*) + c_u \boldsymbol{\beta}_u \mathbf{U}^*,$$

	Setting 1.1	Setting 1.2	Setting 1.3
Modality 1	94.18 (1.69)	180.71 (2.71)	206.44 (3.00)
Modality 2	64.56 (1.30)	256.50 (4.51)	256.50 (4.51)
Early Fusion	5.38 (0.09)	64.37 (1.07)	122.78 (1.97)
Late Fusion	41.98 (0.68)	161.04 (2.66)	185.83 (2.98)
Coop	5.45 (0.09)	109.53 (1.72)	139.14 (2.30)
Meta Fusion	<b>5.07 (0.08)</b>	<b>38.51 (0.64)</b>	<b>49.59 (0.84)</b>

Table 1: Performance of Meta Fusion and benchmarks under Setting 1.1-1.3. Numbers in bold highlight mean MSE values within 1 SE of the lowest MSE across all methods.

where  $\mathbf{X}^*$  and  $\mathbf{Z}^*$  are modality-specific latent covariates,  $\mathbf{S}^*$  represents shared information, and  $\mathbf{U}^*$  captures interaction. See Appendix A1.2 for the full details on generating these variables. Here,  $\beta_t$  ( $t \in \{x, z, s, u\}$ ) denotes the coefficient vector,  $f_t(\cdot)$  is an element-wise transformation function, and  $c_t$  is the component weight.

Let  $p_x$  and  $p_z$  denotes the dimensions of the observed feature, and let  $\mathbf{T}_x$  and  $\mathbf{T}_z$  be the linear mappings to the desired output dimension. Observed features are generated from a signal-plus-noise model:

$$\mathbf{X} = (1 - r_x)[\mathbf{X}^*, \mathbf{S}^*]\mathbf{T}_x + r_x \boldsymbol{\epsilon}_x; \quad \mathbf{Z} = (1 - r_z)[\mathbf{Z}^*, \mathbf{S}^*]\mathbf{T}_z + r_z \boldsymbol{\epsilon}_z,$$

where  $[\cdot, \cdot]$  denotes column-wise concatenation,  $r_x$  and  $r_z \in [0, 1]$  specify the noise ratios, and  $\boldsymbol{\epsilon}_x$  and  $\boldsymbol{\epsilon}_z$  are independent noise matrices.

## 5.1 Complementary modalities

We consider scenarios where the modalities provide complementary information or contain interactions, such that the outcome variable depends jointly on both modalities. For such problems, early fusion strategies are expected to outperform late fusion approaches. Here, we examine three settings with increasing complexities:

- **Setting 1.1:** Linear setting with  $c_x = c_z = 1$ ,  $c_s = c_u = 0$ ;  $f_x$  and  $f_z$  are identity functions; latent dimensions:  $p_x^* = 20$ ,  $p_z^* = 30$ ; observed dimensions:  $p_x = 500$ ,  $p_z = 400$ ; noise ratios:  $r_x = r_z = 0.4$ .
- **Setting 1.2:** Nonlinear setting with  $c_x = c_z = c_u = 1$ ,  $c_s = 0$ ;  $f_x(\mathbf{X}) = \mathbf{X}^2 - \mathbf{X}$  and  $f_z$  is the identity function. Latent dimensions:  $p_x^* = p_z^* = 20$ ; observed dimensions:  $p_x = 2000$ ,  $p_z = 100$ ; noise ratios:  $r_x = 0.1$ ,  $r_z = 0.1$ .
- **Setting 1.3:** Same as Setting 1.2, but with increased noise in the first modality:  $r_x = 0.5$ .

For each setting, we have generated 100 datasets. Table 1 presents the results averaged over these 100 repetitions. As expected, early fusion consistently outperforms late fusion across all settings due to the complementary nature of the modalities. In Setting 1.1, Cooperative

	Setting 2.1	Setting 2.2	Setting 2.3
Modality 1	5.30 (0.14)	75.23 (2.17)	113.93 (2.86)
Modality 2	4.33 (0.10)	64.68 (1.88)	64.69 (1.88)
Early Fusion	2.67 (0.06)	71.57 (2.07)	100.05 (2.59)
Late Fusion	2.70 (0.07)	59.35 (1.75)	74.75 (2.02)
Coop	2.71 (0.07)	58.17 (1.63)	73.94 (1.93)
Meta Fusion	<b>2.47 (0.06)</b>	<b>52.27 (1.35)</b>	<b>53.38 (1.40)</b>

Table 2: Performance of Meta Fusion and benchmarks under Setting 2.1-2.3. Numbers in bold highlight mean MSE values within 1 SE of the lowest MSE across all methods.

Learning (Coop) achieves comparable performance to early fusion by selecting an appropriate disagreement penalty. Meta Fusion, utilizing PCA-generated latent representations and the cohort construction from Section 3.1.1, surpasses early fusion via adaptive mutual learning and top-performer aggregation. Setting 1.2 introduces nonlinearity and dimensional disparity between  $\mathbf{X}$  and  $\mathbf{Z}$ . While early fusion preserves all relevant information, it becomes less efficient due to modality heterogeneity. Meta Fusion, by exploring diverse student cohorts with various latent representation combinations, automatically identifies the most efficient representations, significantly outperforming benchmarks. Setting 1.3 increases the noise in  $\mathbf{X}$ , resulting in an even larger performance gap in favor of Meta Fusion. Notably, Meta Fusion also consistently exhibits smaller standard errors, demonstrating its robustness to noisy and heterogeneous modalities.

## 5.2 Independent modalities

This section explores scenarios where each modality independently contains sufficient information to predict the outcome variable. For such cases, Late Fusion is expected to outperform Early Fusion due to the independent nature of the modalities. We examine three settings with fixed  $c_x = c_z = c_u = 0$ , and  $c_s = 1$ :

- **Setting 2.1:** Linear setting with  $f_s$  as the identity function; latent dimensions:  $p_x^* = 50, p_z^* = 30, p_s^* = 20$ ; observed dimensions:  $p_x = 500, p_z = 400$ ; noise ratios:  $r_x = r_z = 0.4$ .
- **Setting 2.2:** Nonlinear setting with  $f_s(\mathbf{X}) = \mathbf{X}^2 - \mathbf{X}$ ; latent dimensions:  $p_x^* = 50, p_z^* = 30, p_s^* = 20$ ; observed dimensions:  $p_x = 2000, p_z = 400$ ; noise ratios:  $r_x = 0.3, r_z = 0.3$ .
- **Setting 2.3:** Same as Setting 1.2, but with increased noise in the first modality:  $r_x = 0.5$ .

Results in Table 2 are averaged over 100 repetitions. In Setting 2.1, a simple linear scenario, all benchmarks including Early Fusion perform well due to the absence of overfitting issues. Meta Fusion still outperforms other methods by effectively aggregating all students in the cohort. Setting 2.2 introduces nonlinearity and increased noise, causing Early Fu-

sion’s performance to decline. Coop successfully interpolates between Early and Late Fusion paradigms through its disagreement penalty, achieving comparable performance to Late Fusion. Notably, with moderate noise in the first modality, Late Fusion outperforms unimodal predictors. In Setting 2.3, as noise in the first modality increases further, Late Fusion’s performance drops below that of the unimodal predictor trained on the cleaner second modality. However, Meta Fusion maintains its superior performance, significantly outperforming unimodal predictors. This highlights Meta Fusion’s ability to automatically determine what to fuse in the presence of noisy modalities.

In Appendix A3.1, we use the above settings to conduct an ablation study that further investigate the two key components of Meta Fusion: adaptive mutual learning and ensemble learning.

## 6 Real data applications

In this section, we provide two real-data applications to illustrate the utility of our method in practice.

### 6.1 Alzheimer’s disease detection

The rising prevalence of Alzheimer’s disease (AD) poses a significant challenge to healthcare systems worldwide. There is an urgent need for developing efficient and accurate early detection methods. Timely diagnosis not only allows for better patient care and management but also potentially slows disease progression through early interventions. To this end, we apply Meta Fusion to analyze multimodal data from the National Alzheimer’s Coordinating Center (NACC) [44, 45] dataset, aiming to enhance AD detection efficiency and accuracy. The NACC dataset includes four distinct modalities: 1. *Patient Profile* which encompasses demographic information, health history, and family medical background. 2. *Behavioral Assessment* which involves survey questions that gauge the patient’s emotional state, daily functioning, and socioeconomic challenges. 3. *Clinical Evaluation* which consists of more in-depth examinations, including neurological tests (e.g., The Mini Mental State Examination [46]) and physical assessments, conducted by healthcare professionals. 4. *MRI* which includes the summary statistics of the MRI scan, such as hippocampus and gray matter volume. The goal is to integrate these data modalities in order to classify patients into four cognitive status categories: normal cognition, mild cognitive impairment (MCI), impairment but not meeting the MCI criteria, and dementia.

Figure 3 summarizes the classification performance for single-modal classifiers and fusion methods. We exclude cooperative learning from this comparison due to its undefined extension to multi-class classification and lack of clear formulation for more than two modalities, as discussed in Section 2.1. Our analysis, consistent with existing research, shows that behavioral assessments and clinical evaluations are most predictive for Alzheimer’s disease detection [47, 48]. MRI data, while capable of detecting structural brain changes, may not reveal early-stage cognitive decline [49]. Similarly, patient profiles indicate risk factors but may not directly reflect current cognitive status [50].

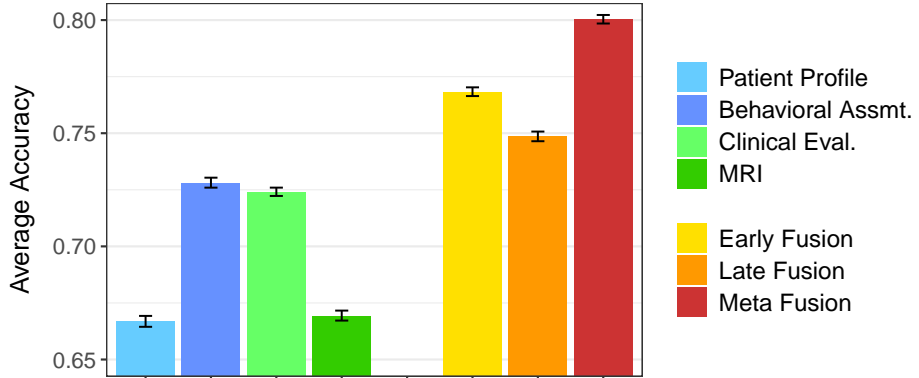


Figure 3: Average accuracy of Meta Fusion and benchmarks on the NACC dataset. Error bars indicate the standard errors. Results are summarized over 100 repetitions.

While all fusion frameworks benefit from integrating multimodal data, the efficacy of conventional fusion benchmarks could be compromised by less-informative modalities. In contrast, Meta Fusion uses supervised encoders [51] to extract latent representations of each modality at different abstraction levels. By carefully selecting and combining powerful latent representations, Meta Fusion maximizes each modality’s contribution, substantially outperforming other benchmarks.

## 6.2 Neural decoding

It is well established that temporal organization is critical to memory and underlies a wide range of perceptual, cognitive, and motor processes [52, 53]. While significant progress has been made in understanding how the brain encodes the spatial context of memories, our knowledge of their temporal organization remains comparatively limited. Recent electrophysiological studies have begun to address this gap (reviewed in [54]), typically by analyzing spike trains, which are sequences of action potentials generated by neurons, and local field potentials (LFPs), which reflect the summed electrical activity in the vicinity of recording electrodes [55]. Effectively integrating these dynamic, multimodal signals is essential for advancing our understanding of the neural mechanisms underlying temporal memory. To this end, we apply Meta Fusion to data collected from a novel experiment, where neural activity was recorded from the CA1 region of the hippocampus as rats performed a nonspatial sequential memory task [56, 57].

The task involves the presentation of repeated sequences of odors at a single port and tests the rats’ ability to identify each odor as “in sequence” (InSeq; by holding their nosepoke response until the signal at 1.2s) or “out of sequence” (OutSeq; by withdrawing their nose before the signal). Spiking and LFP activity was recorded using 24 tetrodes (bundles of 4 electrodes) in rats tested on sequences of 5 odors. For each odor presentation (trial), the data typically features spike counts from  $\sim$ 40-70 neurons, LFP signals from 24 channels (one per tetrode), and trial identifiers (e.g., Odor presented, InSeq/OutSeq, response correct/incorrect).

Most electrophysiological studies primarily focus on spike data for decoding, as it is generally

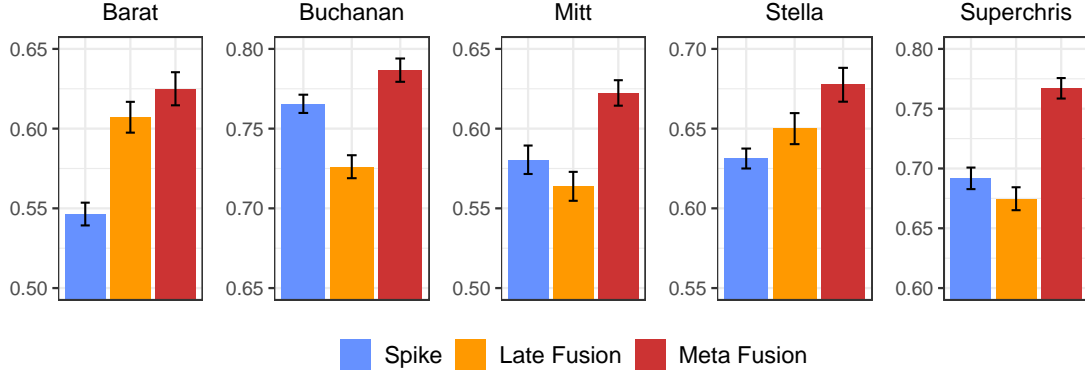


Figure 4: Classification accuracy of Meta Fusion and top benchmarks (Spike-only and Late Fusion) on the memory task for all five rats. Error bars indicate the standard errors. Results are summarized over 100 repetitions.

considered more informative. However, we hypothesize that incorporating both spike and LFP data could provide a more comprehensive view of hippocampal activity and potentially enhance decoding accuracy. We compare Meta Fusion’s performance to that of unimodal predictors and fusion benchmarks in predicting the presented odor from the observed neural signals. Figure 4 summarizes the classification accuracies among the five rats participated in the experiment. We focus on the three top performers: Meta Fusion, Late Fusion, and the unimodal classifier trained only on spike data. As expected, the LFP-only classifier performs poorly. Moreover, Early Fusion’s performance is hindered by the less informative LFP data, which tends to overshadow the cleaner signals in spike data during raw modality fusion. Therefore, we focus our analysis on the top three methods. For a complete comparison of all benchmarks, see the supplementary tables and figures in Appendix A5.

Figure 4 shows varying performance patterns among the five rats. For rats Barat and Stella, Late Fusion outperforms the spike-only classifier, indicating benefits in incorporating the LFP modality. However, for the remaining three rats, particularly Buchanan, Late Fusion performs poorly, suggesting that complete removal of the LFP dataset might be in fact beneficial in some cases. This variability across subjects underscores the need for a fully data-driven, adaptive fusion framework, as no single approach can accommodate individual differences in neural patterns. Meta Fusion successfully adapts to these individual variations, consistently demonstrating strong performance and eliminating the need for human intervention in selecting the appropriate modality or optimal method for latent information extraction.

## 7 Discussion

This paper introduces Meta Fusion, a novel framework for effective integration of diverse data modalities. To address the challenges posed by heterogeneous modalities with varying informational value, Meta Fusion employs a fully data-driven three-step approach. Importantly, the proposed framework unifies existing data fusion paradigms as special cases. Meta

Fusion’s task-agnostic and model-agnostic nature ensures its broad applicability to diverse multimodal fusion tasks.

Our work opens several new directions for future research. The current framework could be extended to handle missing modalities without requiring imputation, both during training and testing. Consider a bimodal dataset comprising one readily available modality and another that is sparsely observed. The model could be trained sequentially: initially, all students are trained on fully observed (complete) samples from both modalities. Once these are exhausted, we continue with unimodal students only, using samples with partially missing data. The soft information sharing mechanism could also be adapted to accommodate this sequential training. During the inference phase, for test data with missing modality, predictions could be aggregated from a subset of student models that utilize only the available modality. This way, our approach can offer a versatile solution for real-world scenarios where complete multimodal data are often difficult to obtain.

The Meta Fusion framework can also be repurposed beyond the multimodal fusion context, presenting promising opportunities for extension to privacy-preserving distributed learning scenarios, particularly in federated learning (FL) contexts. Each student in the cohort could represent a local model with its private dataset, aligning with FL’s decentralized nature [58]. Meta Fusion’s soft information sharing mechanism, which only exchanges predictions, could be adapted to guide local models towards mutual alignment while preserving data privacy. The resulting ensemble could serve as a robust global model, effectively capturing diverse local distributions without compromising individual data security.

## References

- [1] H. Rashed, M. Ramzy, V. Vaquero, A. El Sallab, G. Sistu, and S. Yogamani. “FuseMODNet: Real-Time Camera and LiDAR Based Moving Object Detection for Robust Low-Light Autonomous Driving”. In: *Proceedings of the IEEE/CVF International Conference on Computer Vision (ICCV) Workshops*. Oct. 2019.
- [2] J. Kocić, N. Jovičić, and V. Drndarević. “Sensors and Sensor Fusion in Autonomous Vehicles”. In: *2018 26th Telecommunications Forum (TELFOR)*. 2018, pp. 420–425.
- [3] A. Bagher Zadeh, P. P. Liang, S. Poria, E. Cambria, and L.-P. Morency. “Multimodal Language Analysis in the Wild: CMU-MOSEI Dataset and Interpretable Dynamic Fusion Graph”. In: *Proceedings of the 56th Annual Meeting of the Association for Computational Linguistics (Volume 1: Long Papers)*. Ed. by I. Gurevych and Y. Miyao. Melbourne, Australia: Association for Computational Linguistics, July 2018, pp. 2236–2246.
- [4] R. Das and T. D. Singh. “Multimodal Sentiment Analysis: A Survey of Methods, Trends, and Challenges”. In: *55.13s* (July 2023).
- [5] A. Gandhi, K. Adhvaryu, S. Poria, E. Cambria, and A. Hussain. “Multimodal sentiment analysis: A systematic review of history, datasets, multimodal fusion methods, applications, challenges and future directions”. In: *Information Fusion* 91 (2023), pp. 424–444.
- [6] D. Zhang, Y. Wang, L. Zhou, H. Yuan, and D. Shen. “Multimodal classification of Alzheimer’s disease and mild cognitive impairment”. In: *NeuroImage* 55.3 (2011), pp. 856–867.
- [7] S. Qiu, M. I. Miller, P. S. Joshi, J. C. Lee, C. Xue, Y. Ni, Y. Wang, I. De Andrade Duran, P. H. Hwang, J. A. Cramer, B. C. Dwyer, H. Hao, M. C. Kaku, S. Kedar, P. H. Lee, A. Z. Mian, D. L. Murman, S. O’Shea, A. B. Paul, M.-H. Saint-Hilaire, E. Alton Sartor, A. R. Saxena, L. C. Shih, J. E. Small, M. J. Smith, A. Swaminathan, C. E. Takahashi, O. Taraschenko, H. You, J. Yuan, Y. Zhou, S. Zhu, M. L. Alosco, J. Mez, T. D. Stein, K. L. Poston, R. Au, and V. B. Kolachalama. “Multimodal deep learning for Alzheimer’s disease dementia assessment”. In: *Nature Communications* 13.1 (June 2022).
- [8] S.-C. Huang, A. Pareek, S. Seyyedi, I. Banerjee, and M. P. Lungren. “Fusion of medical imaging and electronic health records using deep learning: a systematic review and implementation guidelines”. In: *npj Digital Medicine* 3.1 (Oct. 2020).
- [9] Y. Zhang, D. Sidibé, O. Morel, and F. Mériadeau. “Deep multimodal fusion for semantic image segmentation: A survey”. In: *Image and Vision Computing* 105 (2021), p. 104042.
- [10] C. Couprie, C. Farabet, L. Najman, and Y. LeCun. “Indoor Semantic Segmentation using depth information”. In: *arXiv: Computer Vision and Pattern Recognition* (2013).
- [11] Y. Xiao, F. Codevilla, A. Gurram, O. Urfalioglu, and A. M. López. “Multimodal End-to-End Autonomous Driving”. In: *Trans. Intell. Transport. Sys.* 23.1 (Jan. 2022), pp. 537–547.

[12] S. Qiu, G. H. Chang, M. Panagia, D. M. Gopal, R. Au, and V. B. Kolachalama. “Fusion of deep learning models of MRI scans, Mini-Mental State Examination, and logical memory test enhances diagnosis of mild cognitive impairment”. In: *Alzheimers Dement (Amst)* 10.1 (Jan. 2018), pp. 737–749.

[13] I. Reda, A. Khalil, M. Elmogy, A. Abou El-Fetouh, A. Shalaby, M. Abou El-Ghar, A. Elmaghhraby, M. Ghazal, and A. El-Baz. “Deep Learning Role in Early Diagnosis of Prostate Cancer”. In: *Technology in Cancer Research Treatment* 17 (Jan. 2018).

[14] Y. Yoo, L. Y. W. Tang, D. K. B. Li, L. Metz, S. Kolind, A. L. Traboulsee, and R. C. Tam. “Deep learning of brain lesion patterns and user-defined clinical and MRI features for predicting conversion to multiple sclerosis from clinically isolated syndrome”. In: *Computer Methods in Biomechanics and Biomedical Engineering: Imaging & Visualization* 7.3 (2019), pp. 250–259.

[15] D. Y. Ding, S. Li, B. Narasimhan, and R. Tibshirani. “Cooperative learning for multiview analysis”. In: *Proceedings of the National Academy of Sciences* 119.38 (2022), e2202113119.

[16] A. Yala, C. Lehman, T. Schuster, T. Portnoi, and R. Barzilay. “A Deep Learning Mammography-based Model for Improved Breast Cancer Risk Prediction”. In: *Radiology* 292.1 (July 2019), pp. 60–66.

[17] D. Nie, J. Lu, H. Zhang, E. Adeli, J. Wang, Z. Yu, L. Liu, Q. Wang, J. Wu, and D. Shen. “Multi-Channel 3D Deep Feature Learning for Survival Time Prediction of Brain Tumor Patients Using Multi-Modal Neuroimages”. In: *Scientific Reports* 9.1 (Jan. 2019).

[18] Y. Tan, F. Liu, B. Li, Z. Zhang, and B. Zhang. “An Efficient Multi-View Multimodal Data Processing Framework for Social Media Popularity Prediction”. In: *Proceedings of the 30th ACM International Conference on Multimedia*. MM ’22. Lisboa, Portugal: Association for Computing Machinery, 2022, pp. 7200–7204.

[19] N. Srivastava and R. R. Salakhutdinov. “Multimodal Learning with Deep Boltzmann Machines”. In: *Advances in Neural Information Processing Systems*. Ed. by F. Pereira, C. Burges, L. Bottou, and K. Weinberger. Vol. 25. Curran Associates, Inc., 2012.

[20] M. Wu and N. Goodman. “Multimodal generative models for scalable weakly-supervised learning”. In: NIPS’18. Montréal, Canada: Curran Associates Inc., 2018, pp. 5580–5590.

[21] T. M. Sutter, Y. Meng, N. Fortin, J. E. Vogt, B. Shahbaba, and S. Mandt. “Unity by Diversity: Improved Representation Learning in Multimodal VAEs”. In: *Sixth Symposium on Advances in Approximate Bayesian Inference - Non Archival Track*. 2024.

[22] Y. Zhang, T. Xiang, T. M. Hospedales, and H. Lu. “Deep Mutual Learning”. In: *2018 IEEE/CVF Conference on Computer Vision and Pattern Recognition* (2017), pp. 4320–4328.

[23] L. Breiman. “Bagging predictors”. In: *Machine Learning* 24.2 (Aug. 1996), pp. 123–140.

[24] R. Caruana, A. Niculescu-Mizil, G. Crew, and A. Ksikes. “Ensemble selection from libraries of models”. In: *Proceedings of the Twenty-First International Conference on Machine Learning*. ICML '04. Banff, Alberta, Canada: Association for Computing Machinery, 2004, p. 18.

[25] R. Tibshirani. “Regression Shrinkage and Selection via the Lasso”. In: *Journal of the Royal Statistical Society. Series B (Methodological)* 58.1 (1996), pp. 267–288.

[26] C. Buciluă, R. Caruana, and A. Niculescu-Mizil. “Model compression”. In: *Proceedings of the 12th ACM SIGKDD International Conference on Knowledge Discovery and Data Mining*. KDD '06. Philadelphia, PA, USA: Association for Computing Machinery, 2006, pp. 535–541.

[27] G. E. Hinton, O. Vinyals, and J. Dean. “Distilling the Knowledge in a Neural Network”. In: *ArXiv* abs/1503.02531 (2015).

[28] Y. Zhang, J. Yang, J. Tian, Z. Shi, C. Zhong, Y. Zhang, and Z. He. “Modality-Aware Mutual Learning for Multi-modal Medical Image Segmentation”. In: *Medical Image Computing and Computer Assisted Intervention – MICCAI 2021: 24th International Conference, Strasbourg, France, September 27–October 1, 2021, Proceedings, Part I*. Strasbourg, France: Springer-Verlag, 2021, pp. 589–599.

[29] J. Wang, J. Li, Y. Shi, J. Lai, and X. Tan. “AM<sup>3</sup>Net: Adaptive Mutual-Learning-Based Multimodal Data Fusion Network”. In: *IEEE Transactions on Circuits and Systems for Video Technology* 32.8 (2022), pp. 5411–5426.

[30] S. Zhang, J. Zhang, B. Tian, T. Lukasiewicz, and Z. Xu. “Multi-modal contrastive mutual learning and pseudo-label re-learning for semi-supervised medical image segmentation”. In: *Medical Image Analysis* 83 (2023), p. 102656.

[31] J. Li, C. Yang, G. Ye, and Q. V. H. Nguyen. “Graph neural networks with deep mutual learning for designing multi-modal recommendation systems”. In: *Information Sciences* 654 (2024), p. 119815.

[32] K. He, X. Zhang, S. Ren, and J. Sun. “Deep Residual Learning for Image Recognition”. In: *2016 IEEE Conference on Computer Vision and Pattern Recognition (CVPR)* (2015), pp. 770–778.

[33] J. Devlin, M.-W. Chang, K. Lee, and K. Toutanova. “BERT: Pre-training of Deep Bidirectional Transformers for Language Understanding”. In: *North American Chapter of the Association for Computational Linguistics*. 2019.

[34] D. Wood, T. Mu, A. M. Webb, H. W. J. Reeve, M. Luján, and G. Brown. “A unified theory of diversity in ensemble learning”. In: *J. Mach. Learn. Res.* 24.1 (Mar. 2024).

[35] A. Kumar and J. Yadav. “A review of feature set partitioning methods for multi-view ensemble learning”. In: *Information Fusion* 100 (2023), p. 101959.

[36] P. J. Rousseeuw. “Silhouettes: A graphical aid to the interpretation and validation of cluster analysis”. In: *Journal of Computational and Applied Mathematics* 20 (1987), pp. 53–65.

[37] D. Marutho, S. Hendra Handaka, E. Wijaya, and Muljono. “The Determination of Cluster Number at k-Mean Using Elbow Method and Purity Evaluation on Headline News”. In: *2018 International Seminar on Application for Technology of Information and Communication*. 2018, pp. 533–538.

[38] R. Caruana, A. Munson, and A. Niculescu-Mizil. “Getting the Most Out of Ensemble Selection”. In: *Sixth International Conference on Data Mining (ICDM’06)*. 2006, pp. 828–833.

[39] K. P. Murphy. *Machine Learning: A Probabilistic Perspective*. The MIT Press, 2012.

[40] A. M. Saxe, J. L. McClelland, and S. Ganguli. “Exact solutions to the nonlinear dynamics of learning in deep linear neural networks”. In: *International Conference on Learning Representations (ICLR)* (2014).

[41] K. Kawaguchi. “Deep Learning without Poor Local Minima”. In: *Advances in Neural Information Processing Systems*. Ed. by D. Lee, M. Sugiyama, U. Luxburg, I. Guyon, and R. Garnett. Vol. 29. Curran Associates, Inc., 2016.

[42] M. Hardt and T. Ma. “Identity Matters in Deep Learning”. In: *International Conference on Learning Representations*. 2017.

[43] M. Phuong and C. H. Lampert. “Towards Understanding Knowledge Distillation”. In: *International Conference on Machine Learning*. 2019.

[44] L. M. Besser, W. A. Kukull, M. A. Teylan, E. H. Bigio, N. J. Cairns, J. K. Kofler, T. J. Montine, J. A. Schneider, and P. T. Nelson. “The Revised National Alzheimer’s Coordinating Center’s Neuropathology Form—Available Data and New Analyses”. In: *Journal of Neuropathology & Experimental Neurology* 77.8 (June 2018), pp. 717–726.

[45] S. Weintraub, L. Besser, H. H. Dodge, M. Teylan, S. Ferris, F. C. Goldstein, B. Giordani, J. Kramer, D. Loewenstein, D. Marson, D. Mungas, D. Salmon, K. Welsh-Bohmer, X.-H. Zhou, S. D. Shirk, A. Atri, W. A. Kukull, C. Phelps, and J. C. Morris. “Version 3 of the Alzheimer Disease Centers’ Neuropsychological Test Battery in the Uniform Data Set (UDS)”. In: *Alzheimer Disease & Associated Disorders* 32.1 (Jan. 2018), pp. 10–17.

[46] M. F. Folstein, S. E. Folstein, and P. R. McHugh. ““Mini-mental state”: A practical method for grading the cognitive state of patients for the clinician”. In: *Journal of Psychiatric Research* 12.3 (1975), pp. 189–198.

[47] S. Weintraub, A. H. Wicklund, and D. P. Salmon. “The Neuropsychological Profile of Alzheimer Disease”. In: *Cold Spring Harbor Perspectives in Medicine* 2.4 (Jan. 2012), a006171–a006171.

[48] K. K. F. Tsoi, J. Y. C. Chan, H. W. Hirai, S. Y. S. Wong, and T. C. Y. Kwok. “Cognitive Tests to Detect Dementia: A Systematic Review and Meta-analysis”. In: *JAMA Internal Medicine* 175.9 (Sept. 2015), p. 1450.

[49] C. R. Jack, D. S. Knopman, W. J. Jagust, L. M. Shaw, P. S. Aisen, M. W. Weiner, R. C. Petersen, and J. Q. Trojanowski. “Hypothetical model of dynamic biomarkers of the Alzheimer’s pathological cascade”. In: *The Lancet Neurology* 9.1 (Jan. 2010), pp. 119–128.

[50] G. Livingston, J. Huntley, A. Sommerlad, D. Ames, C. Ballard, S. Banerjee, C. Brayne, A. Burns, J. Cohen-Mansfield, C. Cooper, S. G. Costafreda, A. Dias, N. Fox, L. N. Gitlin, R. Howard, H. C. Kales, M. Kivimäki, E. B. Larson, A. Ogunniyi, V. Orgeta, K. Ritchie, K. Rockwood, E. L. Sampson, Q. Samus, L. S. Schneider, G. Selbæk, L. Teri, and N. Mukadam. “Dementia prevention, intervention, and care: 2020 report of the Lancet Commission”. In: *The Lancet* 396.10248 (Aug. 2020), pp. 413–446.

[51] M. Trinh, R. Shahbaba, C. Stark, and Y. Ren. “Alzheimer’s disease detection using data fusion with a deep supervised encoder”. In: *Frontiers in Dementia* 3 (Feb. 2024).

[52] E. Tulving. “Episodic and Semantic Memory”. In: *Organization of Memory*. Ed. by E. Tulving and W. Donaldson. New York: Academic Press, 1972, pp. 381–403.

[53] H. Merchant, D. L. Harrington, and W. H. Meck. “Neural basis of the perception and estimation of time”. In: *Annual review of neuroscience* 36 (2013), pp. 313–336.

[54] H. Eichenbaum. “Time cells in the hippocampus: a new dimension for mapping memories.” In: *Nature Reviews Neuroscience* 15 (2014), pp. 732–744.

[55] U. Mitzdorf et al. *Current source-density method and application in cat cerebral cortex: investigation of evoked potentials and EEG phenomena*. American Physiological Society, 1985.

[56] T. A. Allen, D. M. Salz, S. McKenzie, and N. J. Fortin. “Nonspatial sequence coding in CA1 neurons”. In: *Journal of Neuroscience* 36.5 (2016), pp. 1547–1563.

[57] B. Shahbaba, L. Li, F. Agostinelli, M. Saraf, K. W. Cooper, D. Haghverdian, G. A. Elias, P. Baldi, and N. J. Fortin. “Hippocampal ensembles represent sequential relationships among an extended sequence of nonspatial events”. In: *Nature communications* 13.1 (2022), p. 787.

[58] T. Li, A. K. Sahu, A. Talwalkar, and V. Smith. “Federated Learning: Challenges, Methods, and Future Directions”. In: *IEEE Signal Processing Magazine* 37.3 (2020), pp. 50–60.

[59] T.-T. Lu and S.-H. Shiou. “Inverses of  $2 \times 2$  block matrices”. In: *Computers & Mathematics with Applications* 43.1 (2002), pp. 119–129.

## A1 Implementation Details

### A1.1 Extension to multiple modalities

In this section, we describe how to build student cohorts for applications involving more than two modalities. Suppose we have  $M > 2$  modalities  $\mathbf{X}_m \in \mathbb{R}^{n \times p_m}$ , for  $m \in [M]$ , where  $p_m \in \mathbb{Z}$  is the number of features for modality  $\mathbf{X}_m$ . Consider  $k_m \geq 1$  feature extractors for  $\mathbf{X}_m$ , and denote the latent representations, including the null and identity representation, as  $g_m^{i_m}(\mathbf{X}_m)$  for  $i_m \in \{0, \dots, k_m + 1\}$ . We generalize the cross-modal pairing strategy from Section 3.1.1 into a cross-modal matching strategy, forming fused representations from different combinations of unimodal latent representations. Let  $\bigtimes_{m=1}^M \mathcal{S}_m$  denote the cartesian product of sets  $\{\mathcal{S}_m\}_{m \in [M]}$ . There are  $\prod_{m=1}^M (k_m + 2) - 1$  possible nontrivial combinations, which we denote by

$$\mathcal{P} := \left\{ \bigtimes_{m=1}^M \{0, \dots, k_m + 1\} \right\} \setminus \{(0, \dots, 0)\}.$$

For any cross-modal combination  $I = (i_1, \dots, i_M) \in \mathcal{P}$ , the fused representation is  $\bigoplus_{m=1}^M g_m^{i_m}(\mathbf{X}_m)$ . Given a supervised model  $f_I$ , the corresponding student is defined as

$$f_{\Theta_I}(\mathbf{X}_1, \dots, \mathbf{X}_M) := f_I \left( \bigoplus_{m=1}^M g_m^{i_m}(\mathbf{X}_m) \right) \quad (\text{A11})$$

This cross-modal combination strategy explores all possible valid combinations of unimodal latent representations, resulting in a complexity of  $O(\prod_{m=1}^M k_m)$ . Although the number of modalities  $M$  is usually fixed and moderate in most applications, the cohort size can still grow substantially if each modality has many feature extractors. It is worth noting that the construction of the student cohort is flexible and does not need to reach its maximum complexity. If computational costs become prohibitive, it is not necessary to include all possible combinations. Instead, a smaller, more manageable subset can be selected based on domain knowledge.

### A1.2 Details of Synthetic Data Generation

For all simulation studies, we use a latent factor model where the ground-truth label depends on four components: information specific to  $\mathbf{X}$ , information specific to  $\mathbf{Z}$ , shared information, and interaction terms between  $\mathbf{X}$  and  $\mathbf{Z}$ . The data are generated as follows:

1. Represent the latent dimensions for  $\mathbf{X}$ -specific,  $\mathbf{Z}$ -specific, and shared information as  $p_x^*$ ,  $p_z^*$ , and  $p_s^*$ , respectively. Generate latent variables:

$$\begin{aligned} \mathbf{X}^* &\in \mathbb{R}^{n \times p_x^*}, & \mathbf{X}_{ij}^* &\sim N(0, 1); \\ \mathbf{Z}^* &\in \mathbb{R}^{n \times p_z^*}, & \mathbf{Z}_{ij}^* &\sim N(0, 1); \\ \mathbf{S}^* &\in \mathbb{R}^{n \times p_s^*}, & \mathbf{S}_{ij}^* &\sim N(0, 1). \end{aligned}$$

2. Define the interaction terms using the Kronecker product:

$$\mathbf{U}^* \in \mathbb{R}^{n \times p_x^* p_z^*}, \quad \mathbf{U}_i^* = \mathbf{X}_i^* \otimes \mathbf{Z}_i^*,$$

where  $\mathbf{X}_i^*$  and  $\mathbf{Z}_i^*$  are the  $i$ th rows of  $\mathbf{X}^*$  and  $\mathbf{Z}^*$ .

3. Generate the ground-truth label  $\mathbf{Y}$  as:

$$\mathbf{Y} = c_x \boldsymbol{\beta}_x f_x(\mathbf{X}^*) + c_z \boldsymbol{\beta}_z f_z(\mathbf{Z}^*) + c_s \boldsymbol{\beta}_s f_s(\mathbf{S}^*) + c_u \boldsymbol{\beta}_u \mathbf{U}^*,$$

where  $\boldsymbol{\beta}_t$  ( $t \in \{x, z, s, u\}$ ) is the vector of coefficients,  $f_t(\cdot)$  applies an element-wise transformation (e.g., quadratic) to each latent component, and  $c_t$  is the weight that controls the contribution of a specific latent component. For instance, setting  $c_t = 0$  removes that component's influence on  $\mathbf{Y}$ .

4. Let  $p_x$  and  $p_z$  be the observed feature dimensions. The observed features are generated using a signal-plus-noise model based on the latent components:

$$\begin{aligned} \mathbf{X} &= (1 - r_x)[\mathbf{X}^*, \mathbf{S}^*] \mathbf{T}_x + r_x \boldsymbol{\epsilon}_x, \quad \mathbf{T}_x \in \mathbb{R}^{(p_x^* + p_s^*) \times p_x}; \\ \mathbf{Z} &= (1 - r_z)[\mathbf{Z}^*, \mathbf{S}^*] \mathbf{T}_z + r_z \boldsymbol{\epsilon}_z, \quad \mathbf{T}_z \in \mathbb{R}^{(p_z^* + p_s^*) \times p_z}, \end{aligned}$$

where  $[\cdot, \cdot]$  denotes column-wise concatenation,  $r_x, r_z \in [0, 1]$  specify the noise ratios, and  $\boldsymbol{\epsilon}_x$  and  $\boldsymbol{\epsilon}_z$  are noise matrices with entries independently sampled from  $N(0, 1)$ .

### A1.3 Different Ensemble techniques

In addition to the ensemble selection method presented in Algorithm 2, the final prediction can be aggregated using various standard ensemble techniques. Recall that for  $I \in \mathcal{P}$ ,  $\widehat{\mathbf{Y}}_I \in \mathbb{R}^{n \times d}$  denotes the prediction from student model  $f_{\Theta_I}$ , where  $d$  is the output dimension. For instance,  $d = 1$  for regression tasks and  $d = C$  for classification tasks with  $C$  possible classes, where  $\widehat{\mathbf{Y}}_I \in \mathbb{R}^{n \times C}$  denotes the corresponding logits. Below, we present the implementation details of several ensemble alternatives used in our numerical analysis in Appendix A3.1 and Appendix A5. Let  $\mathbf{Y}^{\text{ens}} \in \mathbb{R}^{n \times d}$  denote the final ensemble prediction formulated as follows:

- **Best Single:** This method selects the best performer  $I^*$  among the student cohort based on task-specific loss evaluated on the holdout sample  $\mathcal{D}^{\text{val}}$ . The final prediction is:

$$\mathbf{Y}^{\text{ens}} = \widehat{\mathbf{Y}}_{I^*}$$

- **Stacking:** This method fits an additional supervised model based on stacked outputs of all students. Specifically, recall that  $\bigoplus_{I \in \mathcal{P}} \mathbf{Y}_I$  denotes column-wise concatenation. Let  $f^{\text{ens}}$  denote the supervised model (e.g., a simple DNN model). The final prediction is:

$$\mathbf{Y}^{\text{ens}} = f^{\text{ens}} \left( \bigoplus_{I \in \mathcal{P}} \mathbf{Y}_I \right)$$

- **Simple Average:** This method averages the outputs from all students:

$$\mathbf{Y}^{\text{ens}} = \frac{1}{|\mathcal{P}|} \sum_{I \in \mathcal{P}} \hat{\mathbf{Y}}_I$$

- **Weighted Average:** Given the diversity of the student cohort, a simple average may not be optimal, as the presence of low-performing students could degrade the overall ensemble prediction. Alternatively, one can use a weighted average to dynamically scale the contribution of individual students. Let  $\{w_I\}_{I \in \mathcal{P}}$  be a set of normalized weights that sum to 1. The ensemble prediction is then given by:

$$\mathbf{Y}^{\text{ens}} = \sum_{I \in \mathcal{P}} w_I \hat{\mathbf{Y}}_I,$$

In practice, the weights  $\{w_I\}_{I \in \mathcal{P}}$  are chosen to be proportional to the student's task performance evaluated on the holdout set  $\mathcal{D}^{\text{val}}$ .

For classification tasks, we consider two additional ensemble methods based on voting. Note that  $\hat{\mathbf{Y}}_I \in \mathbb{R}^{n \times C}$  denotes the logits. Let  $\tilde{\mathbf{Y}}_I := \text{argmax}_{c \in [C]} \hat{\mathbf{Y}}_I \in \mathbb{R}^n$  denote the labels predicted by student  $I$ , which finds the largest logit for each sample, and let  $\tilde{\mathbf{Y}}^{\text{ens}}$  denote the label predicted by the ensemble. The two additional ensemble methods are:

- **Majority Vote:** This method determines the most frequent prediction among the student cohort:

$$\tilde{\mathbf{Y}}^{\text{ens}} = \text{argmax}_{c \in [C]} \left( \sum_{I \in \mathcal{P}} \mathbb{I}\{\tilde{\mathbf{Y}}_I = c\} \right)$$

- **Weighted Vote:** Similar to weighted averaging, we can adjust the vote based on weights proportional to each student's performance:

$$\tilde{\mathbf{Y}}^{\text{ens}} = \text{argmax}_{c \in [C]} \left( w_I \sum_{I \in \mathcal{P}} \mathbb{I}\{\tilde{\mathbf{Y}}_I = c\} \right).$$

## A2 Connection to Cooperative Learning

In this section, we show an alternative form of cooperative learning could be viewed as a special case of our proposed framework. Specifically, consider the following simplified objective function of (1) by excluding explicit cross-modal interactions. This simplified objective function is the primary focus in Ding et al. [15].

$$\min_{f_x, f_z} \mathbb{E} \left\{ \frac{1}{2} (Y - f_x(X) - f_z(Z))^2 + \frac{\rho}{2} \|f_x(X) - f_z(Z)\|^2 \right\}, \quad (\text{A12})$$

which has solutions

$$f_x(X) = \mathbb{E} \left\{ \frac{Y}{1 + \rho} - \frac{(1 - \rho)f_z(Z)}{(1 + \rho)} \mid X \right\}, \quad f_z(Z) = \mathbb{E} \left\{ \frac{Y}{1 + \rho} - \frac{(1 - \rho)f_x(X)}{(1 + \rho)} \mid Z \right\}. \quad (\text{A13})$$

To clarify this connection, we consider the population setting used in cooperative learning, as specified in Equation (A12), where the modalities  $X \in \mathbb{R}^{p_x}, Z \in \mathbb{R}^{p_z}$  are treated as random variables. We show that (A12) is a special case of our framework involving two students:  $\widehat{Y}_{\Theta_{k_x+1,0}} := f_{\Theta_{k_x+1,0}}(X, Z)$  that uses  $X$  only, and  $\widehat{Y}_{\Theta_{0,k_z+1}} := f_{\Theta_{0,k_z+1}}(X, Z)$ , that uses  $Z$  only. Denote  $I_x := (k_x + 1, 0)$ , and  $I_z := (0, k_z + 1)$ . We use simple averaging to aggregate predictions. For regression analysis, suppose that both the task loss  $\mathcal{L}$  and the divergence measure  $\mathcal{D}$  are defined based on MSE, and that  $d_{I_x, I_z} = d_{I_z, I_x} = 1$ . In this case, the objective in Equation (4) for the ensemble predictor becomes:

$$\mathcal{L}_{\Theta_{I_x}} = \mathcal{L}_{\Theta_{I_z}} = \mathbb{E} \left\{ \left( Y - \frac{1}{2} (\widehat{Y}_{I_x} + \widehat{Y}_{I_z}) \right)^2 + \rho (\widehat{Y}_{I_z} - \widehat{Y}_{I_x})^2 \right\}, \quad (\text{A14})$$

One can show that the solutions are

$$\widehat{Y}_{I_x} = \mathbb{E} \left\{ \frac{2Y}{1 + \tilde{\rho}} - \frac{(1 - \tilde{\rho})\widehat{Y}_{I_z}}{(1 + \tilde{\rho})} \mid X \right\}, \quad \widehat{Y}_{I_z} = \mathbb{E} \left\{ \frac{2Y}{1 + \tilde{\rho}} - \frac{(1 - \tilde{\rho})\widehat{Y}_{I_x}}{(1 + \tilde{\rho})} \mid Z \right\}, \quad (\text{A15})$$

where  $\tilde{\rho} = 4\rho$  is an adjustable hyperparameter. Consequently, the solutions obtained through cooperative learning in (A13), and the solutions from the alternative implementation of our framework in (A15) result in the same final prediction.

## A3 Additional numerical experiments

### A3.1 Ablation study

This section examines the two key components of Meta Fusion: adaptive mutual learning and ensemble of the student cohort, using the numerical settings in Section 5.2.

To demonstrate the impact of adaptive mutual learning, we compare two key baselines detailed in Appendix A1.3: “Best Single,” which selects the top-performing model from a cohort trained with adaptive mutual learning, and “Best Single (ind.),” which chooses the best model from a cohort trained independently. In Figure A5, Best Single consistently outperforms its independent counterpart, highlighting the efficacy of adaptive mutual learning in enhancing individual model performance within the cohort.

Further, we evaluate several ensemble techniques within our Meta Fusion framework (see Appendix A1.3 for implementation details). While all methods perform similarly in the simple Setting 2.1, the challenging Settings 2.2 and 2.3 reveal key differences. Classical techniques like Stacking and Weighted Average struggle with increased student diversity, often performing worse than the best single model. In contrast, Meta Fusion’s ensemble selection strategy demonstrates robust performance across all settings, effectively handling student heterogeneity in challenging scenarios.

### A3.2 Comparison of Different Divergence Weights

As discussed in Section 3.1.2, incorrectly specified divergence weights can potentially introduce negative knowledge transfer and hinder the effectiveness of mutual learning. In this

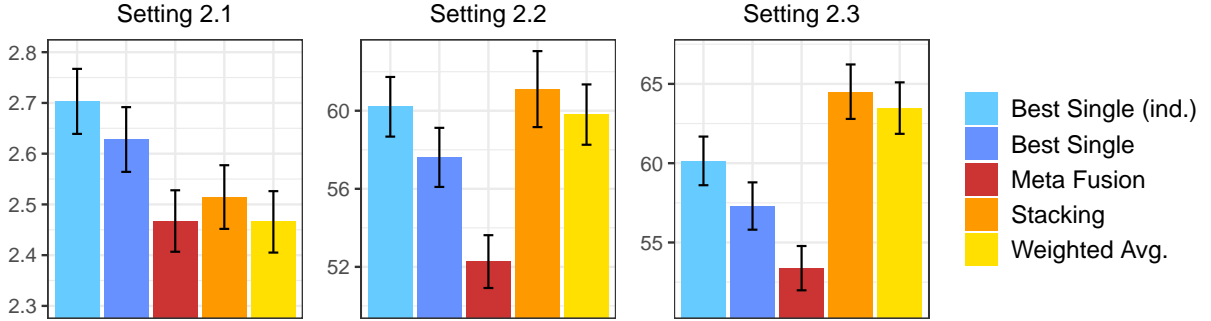


Figure A5: Average MSE of Meta Fusion and ensemble baselines across Settings 2.1-2.3 (Section 5.2). Error bars represent standard errors.

section, we examine the impact of different divergence weights on model performance.

Recall that the divergence weights  $\{d_{I,J}\}_{I,J \in \mathcal{P}, J \neq I}$  in (4) are determined by cluster membership:

$$d_{I,J} = \begin{cases} 1, & \text{if } J \in \mathcal{S}_{\text{top}} \\ 0, & \text{otherwise,} \end{cases}$$

where  $\mathcal{S}_{\text{top}}$  is the set of models belonging to the best-performing  $k_{\text{top}} \geq 1$  clusters with the lowest average initial loss evaluated on the holdout validation set. We investigate the effect of different divergence weights using the neural decoding experiment for one of the rats (Barat, see Section 6.2). Figure A6 illustrates our findings. In all panels, the x-axis represents the latent dimension of the LFP data, while the y-axis represents the latent dimension of spike data. Each grid cell corresponds to a student model with a specific combination of latent representations.

Figure A6a shows the baseline average accuracy of each student in the cohort trained independently (i.e.,  $\rho = 0$  in (4)). Figure A6b displays the accuracy differences (with respect to the baseline) for cohorts trained with different divergence weights, both using  $\rho = 5$ . In the left panel of Figure A6b, we set  $k_{\text{top}} = 1$ , meaning students only learn from  $\mathcal{S}_{\text{top}}$  in the best-performing cluster. Conversely, in the right panel, we define  $\mathcal{S}_{\text{low}}$  as the set of models in the worst-performing cluster and set  $d_{I,J} = 1$  if  $J \in \mathcal{S}_{\text{low}}$  and 0 otherwise, so students only learn from the low performers.

As we can see, both strategies lead to improved individual performances compared to the baseline cohort. However, when students learn from  $\mathcal{S}_{\text{top}}$ , the performance gain is substantially larger than learning from  $\mathcal{S}_{\text{low}}$ . The performance gap between the two sets of divergence weights indicates the presence of negative knowledge transfer when weights are inappropriately specified, which in turn reduces the effectiveness of mutual learning. This underscores the importance of careful weight selection in mutual learning scenarios with heterogeneous student models.

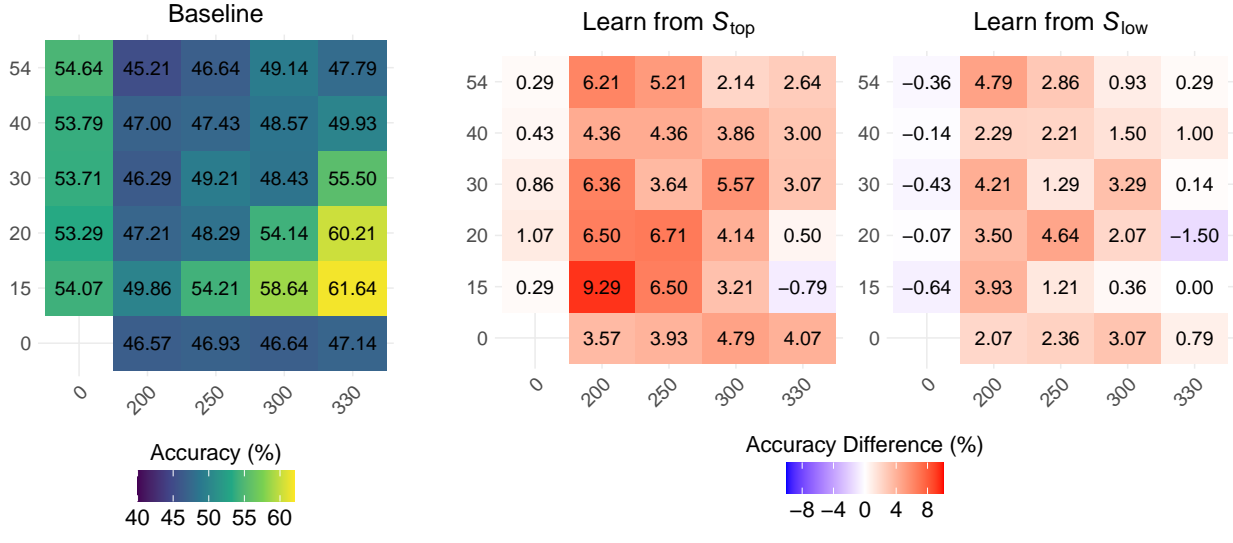


Figure A6: Comparison of student performance trained with different divergence weights for the neural decoding task using Barat’s data (see details in Section 6.2). The results are averaged over 100 experimental repetitions. In all panels, x-axis and y-axis represent latent dimensions of LFP and spike data, respectively. Each grid cell shows a student model with a specific combination of latent representations. (a) shows baseline accuracies of independently trained models without mutual learning. (b) displays accuracy differences relative to the baseline when models learn from the best-performing cluster (left) and the worst-performing cluster (right).

## A4 Proofs

This section presents the proofs of our theoretical results. Appendix A4.2 contains auxiliary technical lemmas, Appendix A4.3 provides detailed proofs for the main theoretical results presented in the manuscript.

### A4.1 Notations

We use the following technical notations:

- For a matrix  $\mathbf{M}$ ,  $\mathbf{M}_i$  denotes the  $i$ -th row and  $\mathbf{M}_{:i}$  denotes the  $i$ -th column.
- For matrices  $\mathbf{M}_I, \mathbf{M}_J$  indexed by  $I, J \in \mathcal{P}$ , we denote  $\mathbf{M}_I^\top \mathbf{M}_J$  as  $\mathbf{M}_{IJ}$  for simplicity.
- For  $\mathbf{x} \in \mathbb{R}^d$ ,  $\mathbf{x}^{\circ 2} := (x_1^2, \dots, x_d^2)$  denotes the element-wise square, and  $\text{Var}^\circ(\mathbf{x}) := (\text{Var}(x_1), \dots, \text{Var}(x_d))$  denotes the element-wise variance.

### A4.2 Additional Technical Results

**Lemma A1.** *Assume the ground truth label  $\mathbf{Y} = (Y_1, \dots, Y_n) \in \mathbb{R}^n$  follows a linear latent factor model  $\mathbf{Y} = \mathbf{V}\boldsymbol{\theta}$  for some coefficients  $\boldsymbol{\theta} \in \mathbb{R}^p$  and latent factors  $\mathbf{V} \in \mathbb{R}^{n \times p}$  according*

to model (6). Assume the fused representation  $\mathbf{V}_I$  and  $\mathbf{V}_J$  satisfy Assumption 1. Let

- $\mathbf{V}_{Ii:}$  and  $\mathbf{V}_{Ji:}$  denote the  $i$ -th row of  $\mathbf{V}_I$  and  $\mathbf{V}_J$ , respectively;
- $\tilde{\Sigma}_I := \mathbf{T}_{II} + \sigma_I^2 \Sigma_I$  and  $\tilde{\Sigma}_J := \mathbf{T}_{JJ} + \sigma_J^2 \Sigma_J$ .

Then  $Y_i$ , for  $i \in [n]$ , can be expressed as:

$$Y_i = \mathbf{V}_{Ii:}^\top \bar{\theta}_I^* + \mathbf{V}_{Ji:}^\top \bar{\theta}_J^* + \bar{\epsilon}_i^*, \quad \bar{\epsilon}_i^* \sim \mathcal{N}(0, \bar{\sigma}^{*2}),$$

where  $\bar{\epsilon}_i^*$  is an independent error term and

$$\begin{aligned} \bar{\theta}_I^* &= (\mathbf{A}^\top \mathbf{T}_I^\top + \mathbf{C}^\top \mathbf{T}_J^\top) \theta, \\ \bar{\theta}_J^* &= (\mathbf{B}^\top \mathbf{T}_I^\top + \mathbf{D}^\top \mathbf{T}_J^\top) \theta, \\ \bar{\sigma}^{*2} &= \theta^\top (\Sigma - (\mathbf{T}_I \mathbf{A} + \mathbf{T}_J \mathbf{C}) \mathbf{T}_I^\top - (\mathbf{T}_I \mathbf{B} + \mathbf{T}_J \mathbf{D}) \mathbf{T}_J^\top) \theta, \end{aligned}$$

where  $\mathbf{A} \in \mathbb{R}^{p_I \times p_I}$ ,  $\mathbf{B} \in \mathbb{R}^{p_I \times p_J}$ ,  $\mathbf{C} \in \mathbb{R}^{p_J \times p_I}$  and  $\mathbf{D} \in \mathbb{R}^{p_J \times p_J}$  satisfies

$$\begin{pmatrix} \mathbf{A} & \mathbf{B} \\ \mathbf{C} & \mathbf{D} \end{pmatrix} = \begin{pmatrix} \tilde{\Sigma}_I & \mathbf{T}_{IJ} \\ \mathbf{T}_{JI} & \tilde{\Sigma}_J \end{pmatrix}^{-1}. \quad (\text{A16})$$

**Remark.** The inverse in (A16) exists since the block matrix on the right hand side is positive definite.

*Proof.* By model (6) and Assumption 1, the latent presentations for each  $i \in [n]$  follows a multivariate Gaussian distribution, namely

$$\begin{pmatrix} \mathbf{V}_{i:} \\ \mathbf{V}_{Ii:} \\ \mathbf{V}_{Ji:} \end{pmatrix} \sim \mathcal{N} \left( \begin{pmatrix} \mathbf{0} \\ \mathbf{0} \\ \mathbf{0} \end{pmatrix}, \begin{pmatrix} \Sigma & \mathbf{T}_I & \mathbf{T}_J \\ \mathbf{T}_I^\top & \tilde{\Sigma}_I & \mathbf{T}_{IJ} \\ \mathbf{T}_J^\top & \mathbf{T}_{JI} & \tilde{\Sigma}_J \end{pmatrix} \right). \quad (\text{A17})$$

The conditional distribution of  $\mathbf{V}_{i:}$  given  $\mathbf{V}_{Ii:}$  and  $\mathbf{V}_{Ji:}$  is still Gaussian with

$$\mathbf{V}_{i:} \mid \mathbf{V}_{Ii:}, \mathbf{V}_{Ji:} \sim \mathcal{N}(\mathbb{E}[\mathbf{V}_{i:} \mid \mathbf{V}_{Ii:}, \mathbf{V}_{Ji:}], \text{Var}[\mathbf{V}_{i:} \mid \mathbf{V}_{Ii:}, \mathbf{V}_{Ji:}]), \quad (\text{A18})$$

where

$$\mathbb{E}[\mathbf{V}_{i:} \mid \mathbf{V}_{Ii:}, \mathbf{V}_{Ji:}] = (\mathbf{T}_I \quad \mathbf{T}_J) \begin{pmatrix} \tilde{\Sigma}_I & \mathbf{T}_{IJ} \\ \mathbf{T}_{JI} & \tilde{\Sigma}_J \end{pmatrix}^{-1} \begin{pmatrix} \mathbf{V}_{Ii:} \\ \mathbf{V}_{Ji:} \end{pmatrix}$$

The inverse in the right hand side always exists since the target covariance matrix is positive definite. Let  $\mathbf{A} \in \mathbb{R}^{p_I \times p_I}$ ,  $\mathbf{B} \in \mathbb{R}^{p_I \times p_J}$ ,  $\mathbf{C} \in \mathbb{R}^{p_J \times p_I}$  and  $\mathbf{D} \in \mathbb{R}^{p_J \times p_J}$  be the matrices satisfying (A16), then we have

$$\begin{aligned} \mathbb{E}[\mathbf{V}_{i:} \mid \mathbf{V}_{Ii:}, \mathbf{V}_{Ji:}] &= (\mathbf{T}_I \quad \mathbf{T}_J) \begin{pmatrix} \mathbf{A} & \mathbf{B} \\ \mathbf{C} & \mathbf{D} \end{pmatrix} \begin{pmatrix} \mathbf{V}_{Ii:} \\ \mathbf{V}_{Ji:} \end{pmatrix} \\ &= (\mathbf{T}_I \mathbf{A} + \mathbf{T}_J \mathbf{C}) \mathbf{V}_{Ii:} + (\mathbf{T}_I \mathbf{B} + \mathbf{T}_J \mathbf{D}) \mathbf{V}_{Ji:} \end{aligned}$$

and

$$\begin{aligned}
\text{Var}[\mathbf{V}_{i:} \mid \mathbf{V}_{Ii:}, \mathbf{V}_{Ji:}] &= \boldsymbol{\Sigma} - (\mathbf{T}_I \quad \mathbf{T}_J) \begin{pmatrix} \tilde{\boldsymbol{\Sigma}}_I & \mathbf{T}_{IJ} \\ \mathbf{T}_{JI} & \tilde{\boldsymbol{\Sigma}}_J \end{pmatrix}^{-1} \begin{pmatrix} \mathbf{T}_I \\ \mathbf{T}_J \end{pmatrix} \\
&= \boldsymbol{\Sigma} - (\mathbf{T}_I \quad \mathbf{T}_J) \begin{pmatrix} \mathbf{A} & \mathbf{B} \\ \mathbf{C} & \mathbf{D} \end{pmatrix} \begin{pmatrix} \mathbf{T}_I \\ \mathbf{T}_J \end{pmatrix} \\
&= \boldsymbol{\Sigma} - (\mathbf{T}_I \mathbf{A} + \mathbf{T}_J \mathbf{C}) \mathbf{T}_I^\top - (\mathbf{T}_I \mathbf{B} + \mathbf{T}_J \mathbf{D}) \mathbf{T}_J^\top.
\end{aligned}$$

Recall that  $Y_i = \mathbf{V}_{i:}^\top \boldsymbol{\theta}$ , hence

$$\begin{aligned}
\mathbb{E}[Y_i \mid \mathbf{V}_{Ii:}, \mathbf{V}_{Ji:}] &= \mathbb{E}[\mathbf{V}_{i:}^\top \boldsymbol{\theta} \mid \mathbf{V}_{Ii:}, \mathbf{V}_{Ji:}] \\
&= \mathbf{V}_{Ii:}^\top (\mathbf{A}^\top \mathbf{T}_I^\top + \mathbf{C}^\top \mathbf{T}_J^\top) \boldsymbol{\theta} + \mathbf{V}_{Ji:}^\top (\mathbf{B}^\top \mathbf{T}_I^\top + \mathbf{D}^\top \mathbf{T}_J^\top) \boldsymbol{\theta},
\end{aligned} \tag{A19}$$

and

$$\begin{aligned}
\text{Var}[Y_i \mid \mathbf{V}_{Ii:}, \mathbf{V}_{Ji:}] &= \text{Var}[\mathbf{V}_{i:}^\top \boldsymbol{\theta} \mid \mathbf{V}_{Ii:}, \mathbf{V}_{Ji:}] \\
&= \boldsymbol{\theta}^\top \text{Var}[\mathbf{V}_{i:} \mid \mathbf{V}_{Ii:}, \mathbf{V}_{Ji:}] \boldsymbol{\theta} \\
&= \boldsymbol{\theta}^\top (\boldsymbol{\Sigma} - (\mathbf{T}_I \mathbf{A} + \mathbf{T}_J \mathbf{C}) \mathbf{T}_I^\top - (\mathbf{T}_I \mathbf{B} + \mathbf{T}_J \mathbf{D}) \mathbf{T}_J^\top) \boldsymbol{\theta}
\end{aligned} \tag{A20}$$

Let

$$\begin{aligned}
\bar{\boldsymbol{\theta}}_I^* &= (\mathbf{A}^\top \mathbf{T}_I^\top + \mathbf{C}^\top \mathbf{T}_J^\top) \boldsymbol{\theta}, \\
\bar{\boldsymbol{\theta}}_J^* &= (\mathbf{B}^\top \mathbf{T}_I^\top + \mathbf{D}^\top \mathbf{T}_J^\top) \boldsymbol{\theta}, \\
\bar{\sigma}^{*2} &= \boldsymbol{\theta}^\top (\boldsymbol{\Sigma} - (\mathbf{T}_I \mathbf{A} + \mathbf{T}_J \mathbf{C}) \mathbf{T}_I^\top - (\mathbf{T}_I \mathbf{B} + \mathbf{T}_J \mathbf{D}) \mathbf{T}_J^\top) \boldsymbol{\theta},
\end{aligned}$$

then combining (A18), (A19) and (A20),  $Y_i$  can be expressed as

$$Y_i = \mathbf{V}_{Ii:}^\top \bar{\boldsymbol{\theta}}_I^* + \mathbf{V}_{Ji:}^\top \bar{\boldsymbol{\theta}}_J^* + \bar{\epsilon}_i^*, \quad \bar{\epsilon}_i^* \sim \mathcal{N}(0, \bar{\sigma}^{*2})$$

where  $\bar{\epsilon}_i^*$  is an independent error term.  $\square$

Lemma A1 characterizes the distribution of  $\mathbf{Y}$  given fused representations  $\mathbf{V}_I, \mathbf{V}_J$  from both students. The following Lemma delineates the conditional distribution of  $\mathbf{Y}$  given only  $\mathbf{V}_I$ .

**Lemma A2.** *Under the same conditions as in Lemma A1,  $Y_i$ , for  $i \in [n]$ , can be alternatively expressed as:*

$$Y_i = \mathbf{V}_{Ii:}^\top \boldsymbol{\theta}_I^* + \epsilon_{Ii}^*, \quad \epsilon_{Ii}^* \sim \mathcal{N}(0, \sigma_I^{*2}),$$

where  $\epsilon_{Ii}^*$  is an error term independent of  $\mathbf{V}_{Ii:}$  and

$$\begin{aligned}
\boldsymbol{\theta}_I^* &= (\tilde{\boldsymbol{\Sigma}}_I)^{-1} \mathbf{T}_I^\top \boldsymbol{\theta}, \\
\sigma_I^{*2} &= \boldsymbol{\theta}^\top (\boldsymbol{\Sigma} - \mathbf{T}_I \tilde{\boldsymbol{\Sigma}}_I^{-1} \mathbf{T}_I^\top) \boldsymbol{\theta},
\end{aligned}$$

*Proof.* By Assumption 1, the joint distribution of  $(\mathbf{V}_{i:}, \mathbf{V}_{Ii:})$ , for  $i \in [n]$  is

$$\begin{pmatrix} \mathbf{V}_{i:} \\ \mathbf{V}_{Ii:} \end{pmatrix} \sim \mathcal{N}\left(\begin{pmatrix} \mathbf{0} \\ \mathbf{0} \end{pmatrix}, \begin{pmatrix} \boldsymbol{\Sigma} & \mathbf{T}_I \\ \mathbf{T}_I^\top & \tilde{\boldsymbol{\Sigma}}_I \end{pmatrix}\right).$$

The conditional distribution of  $\mathbf{V}_{i:}$  given  $\mathbf{V}_{Ii:}$  is still Gaussian with

$$\mathbf{V}_{i:} \mid \mathbf{V}_{Ii:} \sim \mathcal{N}(\mathbb{E}(\mathbf{V}_{i:} \mid \mathbf{V}_{Ii:}), \text{Var}(\mathbf{V}_{i:} \mid \mathbf{V}_{Ii:})), \quad (\text{A21})$$

where

$$\mathbb{E}(\mathbf{V}_{i:} \mid \mathbf{V}_{Ii:}) = \mathbf{T}_I \tilde{\boldsymbol{\Sigma}}_I^{-1} \mathbf{V}_{Ii:}$$

and

$$\text{Var}(\mathbf{V}_{i:} \mid \mathbf{V}_{Ii:}) = \boldsymbol{\Sigma} - \mathbf{T}_I \tilde{\boldsymbol{\Sigma}}_I^{-1} \mathbf{T}_I^\top.$$

Note that the inverse on the right hand side always exist since the target covariance matrix is positive definite. Recall that  $Y_i = \mathbf{V}_{i:}^\top \boldsymbol{\theta}$ , it follows that

$$\mathbb{E}(Y_i \mid \mathbf{V}_{Ii:}) = \mathbb{E}(\mathbf{V}_{i:}^\top \boldsymbol{\theta} \mid \mathbf{V}_{Ii:}) = \mathbf{V}_{Ii:}^\top \tilde{\boldsymbol{\Sigma}}_I^{-1} \mathbf{T}_I^\top \boldsymbol{\theta}, \quad (\text{A22})$$

and

$$\text{Var}(Y_i \mid \mathbf{V}_{Ii:}) = \text{Var}(\mathbf{V}_{i:}^\top \boldsymbol{\theta} \mid \mathbf{V}_{Ii:}) = \boldsymbol{\theta}^\top (\boldsymbol{\Sigma} - \mathbf{T}_I \tilde{\boldsymbol{\Sigma}}_I^{-1} \mathbf{T}_I^\top) \boldsymbol{\theta}. \quad (\text{A23})$$

Let

$$\begin{aligned} \boldsymbol{\theta}_I^* &= \tilde{\boldsymbol{\Sigma}}_I^{-1} \mathbf{T}_I^\top \boldsymbol{\theta}, \\ \sigma_I^{*2} &= \boldsymbol{\theta}^\top (\boldsymbol{\Sigma} - \mathbf{T}_I \tilde{\boldsymbol{\Sigma}}_I^{-1} \mathbf{T}_I^\top) \boldsymbol{\theta}, \end{aligned}$$

by (A21), (A22) and (A23),  $Y_i$  can be expressed as

$$Y_i = \mathbf{V}_{Ii:}^\top \boldsymbol{\theta}_I^* + \epsilon_{Ii}^*, \quad \epsilon_{Ii}^* \sim \mathcal{N}(0, \sigma_I^{*2}),$$

where  $\epsilon_{Ii}^*$  is an error term independent of  $\mathbf{V}_{Ii:}$ . □

**Lemma A3.** *Under the same condition as in Lemma A1, let  $\hat{\boldsymbol{\theta}}_I$  be the fitted estimator given by Proposition 1, the following equalities characterizes the conditional expectation of  $\hat{\boldsymbol{\theta}}_I$  given  $\mathbf{V}_I, \mathbf{V}_J$  and its derivative with respect to  $\rho$  evaluated at  $\rho = 0$ :*

$$\mathbb{E}(\hat{\boldsymbol{\theta}}_I \mid \mathbf{V}_I, \mathbf{V}_J) \mid_{\rho=0} = \bar{\boldsymbol{\theta}}_I^* + \mathbf{V}_{II}^{-1} \mathbf{V}_{IJ} \bar{\boldsymbol{\theta}}_J^*,$$

where  $\bar{\boldsymbol{\theta}}_I^*$  and  $\bar{\boldsymbol{\theta}}_J^*$  are the constants given by Lemma A1. Furthermore

$$\frac{d}{d\rho} \left\{ \mathbb{E}(\hat{\boldsymbol{\theta}}_I \mid \mathbf{V}_I, \mathbf{V}_J) \right\} \mid_{\rho=0} = \mathbf{V}_{II}^{-1} \mathbf{V}_{IJ} \mathbf{V}_{JJ}^{-1} \mathbf{V}_{JI} \bar{\boldsymbol{\theta}}_I^* - \bar{\boldsymbol{\theta}}_I^*.$$

*Proof.* Recall from Proposition 1, the expression of estimator  $\hat{\boldsymbol{\theta}}_I$  can be expanded as

$$\hat{\boldsymbol{\theta}}_I = (1 - \rho) \mathbf{V}_{II}^{-1} \mathbf{V}_I^\top \mathbf{Y} + \rho \mathbf{V}_{II}^{-1} \mathbf{V}_{IJ} \mathbf{V}_{JJ}^{-1} \mathbf{V}_J^\top \mathbf{Y} + \mathbf{H}(\rho),$$

where  $\mathbf{H}(\rho) = \sum_{n=2}^{\infty} \rho^n \mathbf{G}_n$ , for some  $\mathbf{G}_n \in \mathbb{R}^{p_I}$  independent of  $\rho$ . Together with Lemma A1, we have

$$\begin{aligned} \mathbb{E}(\hat{\boldsymbol{\theta}}_I | \mathbf{V}_I, \mathbf{V}_J) |_{\rho=0} &= \mathbb{E}(\mathbf{V}_{II}^{-1} \mathbf{V}_I^\top \mathbf{Y} | \mathbf{V}_I, \mathbf{V}_J) \\ &= \mathbf{V}_{II}^{-1} \mathbf{V}_I^\top \mathbb{E}(\mathbf{Y} | \mathbf{V}_I, \mathbf{V}_J) \\ &= \mathbf{V}_{II}^{-1} \mathbf{V}_I^\top (\mathbf{V}_I \bar{\boldsymbol{\theta}}_I^* + \mathbf{V}_J \bar{\boldsymbol{\theta}}_J^*) \\ &= \mathbf{V}_{II}^{-1} \mathbf{V}_{II} \bar{\boldsymbol{\theta}}_I^* + \mathbf{V}_{II}^{-1} \mathbf{V}_{IJ} \bar{\boldsymbol{\theta}}_J^* \\ &= \bar{\boldsymbol{\theta}}_I^* + \mathbf{V}_{II}^{-1} \mathbf{V}_{IJ} \bar{\boldsymbol{\theta}}_J^* \end{aligned}$$

where  $\bar{\boldsymbol{\theta}}_I^*$  and  $\bar{\boldsymbol{\theta}}_J^*$  are constant vectors given by Lemma A1.

Furthermore, by Leibniz integral rule, we have

$$\begin{aligned} &\frac{d}{d\rho} \left\{ \mathbb{E}(\hat{\boldsymbol{\theta}}_I | \mathbf{V}_I, \mathbf{V}_J) \right\} |_{\rho=0} \\ &= \mathbb{E} \left[ \frac{d}{d\rho} \left\{ (1 - \rho) \mathbf{V}_{II}^{-1} \mathbf{V}_I^\top \mathbf{Y} + \rho \mathbf{V}_{II}^{-1} \mathbf{V}_{IJ} \mathbf{V}_{JJ}^{-1} \mathbf{V}_J^\top \mathbf{Y} + \mathbf{H}(\rho) \right\} |_{\rho=0} | \mathbf{V}_I, \mathbf{V}_J \right] \\ &= \mathbb{E} \left( \mathbf{V}_{II}^{-1} \mathbf{V}_{IJ} \mathbf{V}_{JJ}^{-1} \mathbf{V}_J^\top \mathbf{Y} - \mathbf{V}_{II}^{-1} \mathbf{V}_I^\top \mathbf{Y} | \mathbf{V}_I, \mathbf{V}_J \right) \\ &= \mathbf{V}_{II}^{-1} \mathbf{V}_{IJ} \mathbf{V}_{JJ}^{-1} \mathbf{V}_J^\top (\mathbf{V}_I \bar{\boldsymbol{\theta}}_I^* + \mathbf{V}_J \bar{\boldsymbol{\theta}}_J^*) - \mathbf{V}_{II}^{-1} \mathbf{V}_I^\top (\mathbf{V}_I \bar{\boldsymbol{\theta}}_I^* + \mathbf{V}_J \bar{\boldsymbol{\theta}}_J^*) \\ &= \mathbf{V}_{II}^{-1} \mathbf{V}_{IJ} \mathbf{V}_{JJ}^{-1} \mathbf{V}_{JI} \bar{\boldsymbol{\theta}}_I^* - \bar{\boldsymbol{\theta}}_I^* \end{aligned}$$

□

**Lemma A4.** *Under Assumptions 1 and 2, the following inequality holds.*

$$\Xi := \frac{2\bar{\sigma}^{*2}}{n} \sum_{m=1}^{p_I} \left( \sum_{k=1}^{p_J} \frac{(\mathbf{T}_{J:k}^\top \mathbf{T}_{I:m})^2}{(\mathbf{T}_{I:m}^\top \mathbf{T}_{I:m} + \sigma_I^2)(\mathbf{T}_{J:k}^\top \mathbf{T}_{J:k} + \sigma_J^2)} - 1 \right) < 0,$$

where  $\bar{\sigma}^{*2} > 0$  is a constant as defined in Lemma A1.

*Proof.* Since  $\bar{\sigma}^{*2} > 0$ , it suffices to show that for  $\forall m \in [p_I]$ ,

$$\sum_{k=1}^{p_J} \frac{(\mathbf{T}_{J:k}^\top \mathbf{T}_{I:m})^2}{(\mathbf{T}_{I:m}^\top \mathbf{T}_{I:m} + \sigma_I^2)(\mathbf{T}_{J:k}^\top \mathbf{T}_{J:k} + \sigma_J^2)} < 1.$$

For  $k \in [p_J]$ , let  $\tilde{\mathbf{T}}_{J:k} := \mathbf{T}_{J:k} / \|\mathbf{T}_{J:k}\|$  be the normalized columns of  $\mathbf{T}_J$ , and let  $\tilde{\mathbf{T}}_J$  denote the corresponding normalized matrix. Similarly, For  $m \in [p_I]$ , let  $\tilde{\mathbf{T}}_{I:m} := \mathbf{T}_{I:m} / \|\mathbf{T}_{I:m}\|$  be the

normalized columns of  $\mathbf{T}_I$ , then

$$\begin{aligned}
\sum_{k=1}^{p_J} \frac{(\mathbf{T}_{J:k}^\top \mathbf{T}_{I:m})^2}{(\mathbf{T}_{I:m}^\top \mathbf{T}_{I:m} + \sigma_I^2)(\mathbf{T}_{J:k}^\top \mathbf{T}_{J:k} + \sigma_J^2)} &< \sum_{k=1}^{p_J} \frac{(\mathbf{T}_{J:k}^\top \mathbf{T}_{I:m})^2}{(\mathbf{T}_{I:m}^\top \mathbf{T}_{I:m})(\mathbf{T}_{J:k}^\top \mathbf{T}_{J:k})} \\
&= \sum_{k=1}^{p_J} \tilde{\mathbf{T}}_{J:k}^\top \tilde{\mathbf{T}}_{I:m} \\
&= \|\tilde{\mathbf{T}}_J^\top \tilde{\mathbf{T}}_{I:m}\|^2 \\
&= \tilde{\mathbf{T}}_{I:m}^\top \tilde{\mathbf{T}}_J \tilde{\mathbf{T}}_J^\top \tilde{\mathbf{T}}_{I:m}.
\end{aligned}$$

By Assumption 2,  $p_I, p_J \leq p$  and  $\tilde{\mathbf{T}}_J$  has orthonormal columns. It follows that,  $\tilde{\mathbf{T}}_J$  has a singular value decomposition with  $\tilde{\mathbf{T}}_J = \tilde{\mathbf{U}} \tilde{\mathbf{D}} \tilde{\mathbf{V}}^\top$ , where  $\tilde{\mathbf{U}} \in \mathbb{R}^{p \times p}$ ,  $\tilde{\mathbf{V}} \in \mathbb{R}^{p_J \times p_J}$  are orthogonal matrices and  $\tilde{\mathbf{D}} \in \mathbb{R}^{p \times p_J}$  is a rectangular diagonal matrix whose diagonal entries are all equal to 1. Therefore,

$$\begin{aligned}
\sum_{k=1}^{p_J} \frac{(\mathbf{T}_{J:k}^\top \mathbf{T}_{I:m})^2}{(\mathbf{T}_{I:m}^\top \mathbf{T}_{I:m} + \sigma_I^2)(\mathbf{T}_{J:k}^\top \mathbf{T}_{J:k} + \sigma_J^2)} &< \tilde{\mathbf{T}}_{I:m}^\top \tilde{\mathbf{T}}_J \tilde{\mathbf{T}}_J^\top \tilde{\mathbf{T}}_{I:m} \\
&= \tilde{\mathbf{T}}_{I:m}^\top \tilde{\mathbf{U}} \tilde{\mathbf{D}} \tilde{\mathbf{V}}^\top \tilde{\mathbf{V}} \tilde{\mathbf{D}}^\top \tilde{\mathbf{U}}^\top \tilde{\mathbf{T}}_{I:m} \\
&= \tilde{\mathbf{T}}_{I:m}^\top \tilde{\mathbf{U}} \tilde{\mathbf{D}} \tilde{\mathbf{D}}^\top \tilde{\mathbf{U}}^\top \tilde{\mathbf{T}}_{I:m} \\
&\leq \tilde{\mathbf{T}}_{I:m}^\top \tilde{\mathbf{U}} \tilde{\mathbf{U}}^\top \tilde{\mathbf{T}}_{I:m} \\
&= \|\tilde{\mathbf{T}}_{I:m}\|^2 = 1,
\end{aligned}$$

which concludes the proof.  $\square$

**Lemma A5.** *Under the same condition as in Lemma A1, the following equality holds.*

$$\tilde{\Sigma}_I^{-1} \mathbf{T}_{IJ} \bar{\theta}_J^* - (\theta_I^* - \bar{\theta}_I^*) = \mathbf{0},$$

where  $\theta_I^*$  is a constant defined in Lemma A2, and  $\bar{\theta}_I^*$ ,  $\bar{\theta}_J^*$  are constants given by Lemma A1.

*Proof.* Recall from Lemma A1 and Lemma A2,

$$\begin{aligned}
\theta_I^* &= \tilde{\Sigma}_I^{-1} \mathbf{T}_I^\top \theta, \\
\bar{\theta}_I^* &= (\mathbf{A}^\top \mathbf{T}_I^\top + \mathbf{C}^\top \mathbf{T}_J^\top) \theta, \\
\bar{\theta}_J^* &= (\mathbf{B}^\top \mathbf{T}_I^\top + \mathbf{D}^\top \mathbf{T}_J^\top) \theta,
\end{aligned}$$

where  $\mathbf{A} \in \mathbb{R}^{p_I \times p_I}$ ,  $\mathbf{B} \in \mathbb{R}^{p_I \times p_J}$ ,  $\mathbf{C} \in \mathbb{R}^{p_J \times p_I}$  and  $\mathbf{D} \in \mathbb{R}^{p_J \times p_J}$  satisfies

$$\begin{pmatrix} \mathbf{A} & \mathbf{B} \\ \mathbf{C} & \mathbf{D} \end{pmatrix} = \begin{pmatrix} \tilde{\Sigma}_I & \mathbf{T}_{IJ} \\ \mathbf{T}_{JI} & \tilde{\Sigma}_J \end{pmatrix}^{-1}.$$

Then we must have that

$$\begin{pmatrix} \mathbf{A} & \mathbf{B} \\ \mathbf{C} & \mathbf{D} \end{pmatrix} \begin{pmatrix} \tilde{\Sigma}_I & \mathbf{T}_{IJ} \\ \mathbf{T}_{JI} & \tilde{\Sigma}_J \end{pmatrix} = \begin{pmatrix} \mathbf{A} \tilde{\Sigma}_I + \mathbf{B} \mathbf{T}_{JI} & \mathbf{A} \mathbf{T}_{IJ} + \mathbf{B} \tilde{\Sigma}_J \\ \mathbf{C} \tilde{\Sigma}_I + \mathbf{D} \mathbf{T}_{JI} & \mathbf{C} \mathbf{T}_{IJ} + \mathbf{D} \tilde{\Sigma}_J \end{pmatrix} = \begin{pmatrix} \Sigma_I & \mathbf{0} \\ \mathbf{0} & \Sigma_J \end{pmatrix},$$

where  $\Sigma_I \in \mathbb{R}^{p_I \times p_I}$ ,  $\Sigma_J \in \mathbb{R}^{p_J \times p_J}$  are identity matrices, and  $\mathbf{0}$  represents rectangular block matrix of 0s. It implies that,

$$\begin{aligned}
& (\Sigma_I - \tilde{\Sigma}_I \mathbf{A}^\top - \mathbf{T}_{IJ} \mathbf{B}^\top) \mathbf{T}_I^\top = (\tilde{\Sigma}_I \mathbf{C}^\top + \mathbf{T}_{IJ} \mathbf{D}^\top) \mathbf{T}_J^\top, \\
\implies & \mathbf{T}_I^\top - \tilde{\Sigma}_I \mathbf{A}^\top \mathbf{T}_I^\top - \mathbf{T}_{IJ} \mathbf{B}^\top \mathbf{T}_I^\top = \tilde{\Sigma}_I \mathbf{C}^\top \mathbf{T}_J^\top + \mathbf{T}_{IJ} \mathbf{D}^\top \mathbf{T}_J^\top \\
\implies & \mathbf{T}_I^\top - \mathbf{T}_{IJ} (\mathbf{B}^\top \mathbf{T}_I^\top + \mathbf{D}^\top \mathbf{T}_J^\top) = \tilde{\Sigma}_I (\mathbf{A}^\top \mathbf{T}_I^\top + \mathbf{C}^\top \mathbf{T}_J^\top) \\
\implies & \tilde{\Sigma}_I^{-1} \mathbf{T}_I^\top - \tilde{\Sigma}_I^{-1} \mathbf{T}_{IJ} (\mathbf{B}^\top \mathbf{T}_I^\top + \mathbf{D}^\top \mathbf{T}_J^\top) = \mathbf{A}^\top \mathbf{T}_I^\top + \mathbf{C}^\top \mathbf{T}_J^\top \\
\implies & \tilde{\Sigma}_I^{-1} \mathbf{T}_{IJ} (\mathbf{B}^\top \mathbf{T}_I^\top + \mathbf{D}^\top \mathbf{T}_J^\top) + (\mathbf{A}^\top \mathbf{T}_I^\top + \mathbf{C}^\top \mathbf{T}_J^\top) = \tilde{\Sigma}_I^{-1} \mathbf{T}_I^\top \\
\implies & \tilde{\Sigma}_I^{-1} \mathbf{T}_{IJ} (\mathbf{B}^\top \mathbf{T}_I^\top + \mathbf{D}^\top \mathbf{T}_J^\top) \boldsymbol{\theta} + (\mathbf{A}^\top \mathbf{T}_I^\top + \mathbf{C}^\top \mathbf{T}_J^\top) \boldsymbol{\theta} = \tilde{\Sigma}_I^{-1} \mathbf{T}_I^\top \boldsymbol{\theta} \\
\implies & \tilde{\Sigma}_I^{-1} \mathbf{T}_{IJ} \bar{\boldsymbol{\theta}}_J^* + \bar{\boldsymbol{\theta}}_I^* = \boldsymbol{\theta}_I^*,
\end{aligned}$$

and rearranging the last equality concludes the proof.  $\square$

### A4.3 Proofs of Main Results

*Proof of Proposition 1.* We begin to write down the explicit expression for the fitted parameters  $\hat{\boldsymbol{\theta}}_I, \hat{\boldsymbol{\theta}}_J$ , let

$$\tilde{\boldsymbol{\theta}} = \begin{pmatrix} \boldsymbol{\theta}_I \\ \boldsymbol{\theta}_J \end{pmatrix}, \tilde{\mathbf{V}} = \begin{pmatrix} \mathbf{V}_I & \mathbf{0} \\ \mathbf{0} & \mathbf{V}_J \\ \sqrt{\rho} \mathbf{V}_I & -\sqrt{\rho} \mathbf{V}_J \end{pmatrix}, \tilde{\mathbf{Y}} = \begin{pmatrix} \mathbf{Y} \\ \mathbf{Y} \\ \mathbf{0} \end{pmatrix},$$

where  $\mathbf{0}$  is boldfaced to indicate that it is a zero matrix. Its dimension is left unspecified unless needed for clarity. Note that solving (8) is equivalent to solving

$$\hat{\boldsymbol{\theta}} = \underset{\tilde{\boldsymbol{\theta}}}{\operatorname{argmin}} \|\tilde{\mathbf{Y}} - \tilde{\mathbf{V}} \tilde{\boldsymbol{\theta}}\|^2,$$

when  $n > \max\{p_I, p_J\}$ , the equation above has solution in the form of:

$$\hat{\boldsymbol{\theta}} = \begin{pmatrix} \hat{\boldsymbol{\theta}}_I \\ \hat{\boldsymbol{\theta}}_J \end{pmatrix} = (\tilde{\mathbf{V}}^\top \tilde{\mathbf{V}})^{-1} (\tilde{\mathbf{V}}^\top \tilde{\mathbf{Y}}), \quad (\text{A24})$$

where

$$\begin{aligned}
\tilde{\mathbf{V}}^\top \tilde{\mathbf{V}} &= \begin{pmatrix} \mathbf{V}_I^\top & \mathbf{0} & \sqrt{\rho} \mathbf{V}_I^\top \\ \mathbf{0} & \mathbf{V}_J^\top & -\sqrt{\rho} \mathbf{V}_J^\top \end{pmatrix} \begin{pmatrix} \mathbf{V}_I & \mathbf{0} \\ \mathbf{0} & \mathbf{V}_J \\ \sqrt{\rho} \mathbf{V}_I & -\sqrt{\rho} \mathbf{V}_J \end{pmatrix} \\
&= \begin{pmatrix} (1 + \rho) \mathbf{V}_{II} & -\rho \mathbf{V}_{IJ} \\ -\rho \mathbf{V}_{JI} & (1 + \rho) \mathbf{V}_{JJ} \end{pmatrix},
\end{aligned} \quad (\text{A25})$$

and

$$\tilde{\mathbf{V}}^\top \tilde{\mathbf{Y}} = \begin{pmatrix} \mathbf{V}_I^\top & \mathbf{0} & \sqrt{\rho} \mathbf{V}_I^\top \\ \mathbf{0} & \mathbf{V}_J^\top & -\sqrt{\rho} \mathbf{V}_J^\top \end{pmatrix} \begin{pmatrix} \mathbf{Y} \\ \mathbf{Y} \\ \mathbf{0} \end{pmatrix} = \begin{pmatrix} \mathbf{V}_I^\top \mathbf{Y} \\ \mathbf{V}_J^\top \mathbf{Y} \\ \mathbf{0} \end{pmatrix}. \quad (\text{A26})$$

We first establish the invertibility of  $\tilde{\mathbf{V}}^\top \tilde{\mathbf{V}} \in \mathbb{R}^{(p_I+p_J) \times (p_I+p_J)}$ , then derive a power series expansion of the inverse matrix.

First note that  $\tilde{\mathbf{V}}^\top \tilde{\mathbf{V}}$  in (A25) can be rearranged into

$$\begin{aligned}\tilde{\mathbf{V}}^\top \tilde{\mathbf{V}} &= \begin{pmatrix} (1+\rho)\mathbf{V}_{II} & -\rho\mathbf{V}_{IJ} \\ -\rho\mathbf{V}_{JI} & (1+\rho)\mathbf{V}_{JJ} \end{pmatrix} \\ &= \underbrace{\begin{pmatrix} \mathbf{V}_{II} & 0 \\ 0 & \mathbf{V}_{JJ} \end{pmatrix}}_{:=\mathbf{E}} - \rho \underbrace{\begin{pmatrix} -\mathbf{V}_{II} & \mathbf{V}_{IJ} \\ \mathbf{V}_{JI} & -\mathbf{V}_{JJ} \end{pmatrix}}_{:=\mathbf{F}},\end{aligned}\tag{A27}$$

which isolates the effect of the  $\rho$ . Equivalently, we have  $\tilde{\mathbf{V}}^\top \tilde{\mathbf{V}} = \mathbf{E} + \rho(-\mathbf{F})$ . One can easily show that  $-\mathbf{F}$  is positive semidefinite and  $\mathbf{E}$  is positive definite when  $\mathbf{V}_{II}$  and  $\mathbf{V}_{JJ}$  are both of full rank. Under Assumption 1,  $\mathbf{V}_{II}$  and  $\mathbf{V}_{JJ}$  follow Wishart distribution and are invertible if  $n \geq p_I$  and  $n \geq p_J$ . By definition,  $\rho \geq 0$ , hence,  $\tilde{\mathbf{V}}^\top \tilde{\mathbf{V}} = \mathbf{E} + \rho(-\mathbf{F})$  is positive definite when  $n \geq \max\{p_I, p_J\}$ .

The inverse of  $\tilde{\mathbf{V}}^\top \tilde{\mathbf{V}} \in \mathbb{R}^{(p_I+p_J) \times (p_I+p_J)}$  has a nontrivial analytical solution in high dimensional case. While theoretically, it is possible to derive a closed form of  $\tilde{\mathbf{V}}^\top \tilde{\mathbf{V}}^{-1}$  by applying the general formula of inverting  $2 \times 2$  block matrices [59], the resulting inverse matrix will be a complex expression in terms of  $\rho$  which makes it nearly impossible to conduct the subsequent analysis. Therefore, we derive a power series expansion of  $\tilde{\mathbf{V}}^\top \tilde{\mathbf{V}}$  below.

By Neumann series, inverse of  $\tilde{\mathbf{V}}^\top \tilde{\mathbf{V}}$  can be expanded as a power series

$$\begin{aligned}(\tilde{\mathbf{V}}^\top \tilde{\mathbf{V}})^{-1} &= (\mathbf{E} - \rho\mathbf{F})^{-1} \\ &= (\mathbf{I} - \rho\mathbf{E}^{-1}\mathbf{F})^{-1}\mathbf{E}^{-1} \\ &= \left\{ \sum_{k=0}^{\infty} (\rho\mathbf{E}^{-1}\mathbf{F})^k \right\} \mathbf{E}^{-1} \\ &= \mathbf{E}^{-1} + \rho\mathbf{E}^{-1}\mathbf{F}\mathbf{E}^{-1} + \rho^2\mathbf{E}^{-1}\mathbf{F}\mathbf{E}^{-1}\mathbf{F}\mathbf{E}^{-1} + \mathbf{H}(\rho)\end{aligned}\tag{A28}$$

where  $\mathbf{H}(\rho)$  is the higher order terms of  $\rho$ . Since we will be analyzing how the generalization error changes around  $\rho = 0$ , we focus on the quadratic approximation which dominates the power series. The benefits of the expansion above is that it bypasses the needs of computing the explicit inverse of a general block matrix and we only need to compute the inverse of a sparse matrix  $\mathbf{E}$ , which is simply

$$\mathbf{E}^{-1} = \begin{pmatrix} \mathbf{V}_{II} & 0 \\ 0 & \mathbf{V}_{JJ} \end{pmatrix}^{-1} = \begin{pmatrix} \mathbf{V}_{II}^{-1} & 0 \\ 0 & \mathbf{V}_{JJ}^{-1} \end{pmatrix}\tag{A29}$$

Plugging in (A29) into (A28), we can show with direct computation that the estimator is

$$\hat{\boldsymbol{\theta}}_I = (1 - \rho)\mathbf{V}_{II}^{-1}\mathbf{V}_I^\top \mathbf{Y} + \rho\mathbf{V}_{II}^{-1}\mathbf{V}_{IJ}\mathbf{V}_{JJ}^{-1}\mathbf{V}_J^\top \mathbf{Y} + \mathbf{H}(\rho),$$

where  $\mathbf{H}(\rho) = \sum_{n=2}^{\infty} \rho^n \mathbf{G}_n$ , for some  $\mathbf{G}_n \in \mathbb{R}^{p_I}$  independent of  $\rho$ .  $\square$

*Proof of Theorem 1.* Recall that  $Y_*$  is the ground-truth label of a new test point and  $\mathbf{V}_{I*}$  is the corresponding fused representation for student  $I$ . We begin to examine the MSE of the individual student model. By Lemma A2, we have

$$\text{MSE}(I; \rho) = \mathbb{E}\left\{(Y_* - \mathbf{V}_{I*}^\top \hat{\boldsymbol{\theta}}_I)^2 \mid \mathbf{V}_I\right\} = \mathbb{E}\left[\left\{\mathbf{V}_{I*}^\top (\boldsymbol{\theta}_I^* - \hat{\boldsymbol{\theta}}_I)\right\}^2 \mid \mathbf{V}_I\right] + \sigma_I^{*2}. \quad (\text{A30})$$

The first term in the last equality is

$$\begin{aligned} & \mathbb{E}\left[\left\{\mathbf{V}_{I*}^\top (\boldsymbol{\theta}_I^* - \hat{\boldsymbol{\theta}}_I)\right\}^2 \mid \mathbf{V}_I\right] \\ &= \mathbb{E}\left[\left\{\sum_{i=1}^{p_I} V_{I*i}(\theta_{Ii}^* - \hat{\theta}_{Ii})\right\}^2 \mid \mathbf{V}_I\right] \\ &= \sum_{i=1}^{p_I} \mathbb{E}\left\{V_{I*i}^2(\theta_{Ii}^* - \hat{\theta}_{Ii})^2 \mid \mathbf{V}_I\right\} + 2 \sum_{1 \leq i < j \leq p_I} \mathbb{E}\left\{V_{I*i} V_{I*j} (\theta_{Ii}^* - \hat{\theta}_{Ii})(\theta_{Ij}^* - \hat{\theta}_{Ij}) \mid \mathbf{V}_I\right\} \\ &= \sum_{i=1}^{p_I} \mathbb{E}(V_{I*i}^2) \mathbb{E}\left\{(\theta_{Ii}^* - \hat{\theta}_{Ii})^2 \mid \mathbf{V}_I\right\} + 2 \sum_{1 \leq i < j \leq p_I} \mathbb{E}(V_{I*i} V_{I*j}) \mathbb{E}\left\{(\theta_{Ii}^* - \hat{\theta}_{Ii})(\theta_{Ij}^* - \hat{\theta}_{Ij}) \mid \mathbf{V}_I\right\}, \end{aligned}$$

by Assumption 2 which implies features are mutually independent, the second term in the last equality vanishes, together with (A17) in Lemma A1, we have

$$\begin{aligned} & \mathbb{E}\left[\left\{\mathbf{V}_{I*}^\top (\boldsymbol{\theta}_I^* - \hat{\boldsymbol{\theta}}_I)\right\}^2 \mid \mathbf{V}_I\right] \\ &= \sum_{i=1}^{p_I} \mathbb{E}(V_{I*i}^2) \mathbb{E}\left\{(\theta_{Ii}^* - \hat{\theta}_{Ii})^2 \mid \mathbf{V}_I\right\} \\ &= \sum_{i=1}^{p_I} \mathbb{E}(V_{I*i}^2) \text{Var}\left\{(\theta_{Ii}^* - \hat{\theta}_{Ii})^2 \mid \mathbf{V}_I\right\} + \sum_{i=1}^{p_I} \mathbb{E}(V_{I*i}^2) \left\{\mathbb{E}\left(\theta_{Ii}^* - \hat{\theta}_{Ii} \mid \mathbf{V}_I\right)\right\}^2 \\ &= \underbrace{\text{diag}\left(\tilde{\boldsymbol{\Sigma}}_I\right)^\top \text{Var}^\circ\left(\hat{\boldsymbol{\theta}}_I \mid \mathbf{V}_I\right)}_{:=V(\mathbf{V}_I; \rho)} + \underbrace{\text{diag}\left(\tilde{\boldsymbol{\Sigma}}_I\right)^\top \left\{\mathbb{E}\left(\boldsymbol{\theta}_I^* - \hat{\boldsymbol{\theta}}_I \mid \mathbf{V}_I\right)\right\}^{\circ 2}}_{:=B^2(\mathbf{V}_I; \rho)}, \end{aligned} \quad (\text{A31})$$

where for vector  $\mathbf{x} = (x_1, \dots, x_n)$ ,  $\text{Var}^\circ(\mathbf{x}) = (\text{Var}(x_1), \dots, \text{Var}(x_n))$  denotes the element-wise variance and  $\mathbf{x}^{\circ 2} = (x_1^2, \dots, x_n^2)$  denotes the element-wise square.

Combining (A30) and (A31), we have that

$$\text{MSE}(I; \rho) = V(\mathbf{V}_I; \rho) + B^2(\mathbf{V}_I; \rho) + \sigma_I^{*2}, \quad (\text{A32})$$

where  $V(\mathbf{V}_I; \rho)$  is the variance related term and  $B^2(\mathbf{V}_I; \rho)$  is the bias related term.

We first inspect how  $B^2(\mathbf{V}_I; \rho)$  change with respect to  $\rho$ ,

$$\begin{aligned} \frac{d}{d\rho} B^2(\mathbf{V}_I; \rho) &= \frac{d}{d\rho} \left[ \text{diag}\left(\tilde{\boldsymbol{\Sigma}}_I\right)^\top \left\{\mathbb{E}\left(\boldsymbol{\theta}_I^* - \hat{\boldsymbol{\theta}}_I \mid \mathbf{V}_I\right)\right\}^{\circ 2} \right] \\ &= 2 \text{diag}\left(\tilde{\boldsymbol{\Sigma}}_I\right)^\top \left[ \mathbb{E}\left\{(\boldsymbol{\theta}_I^* - \hat{\boldsymbol{\theta}}_I) \mid \mathbf{V}_I\right\} \circ \frac{d}{d\rho} \mathbb{E}\left\{(\boldsymbol{\theta}_I^* - \hat{\boldsymbol{\theta}}_I) \mid \mathbf{V}_I\right\} \right], \end{aligned}$$

where  $\mathbf{x} \circ \mathbf{y}$  denotes the Hadamard product of two vectors  $\mathbf{x}$  and  $\mathbf{y}$ . Recall from Proposition 1, the fitted estimator  $\hat{\boldsymbol{\theta}}_I$  is

$$\hat{\boldsymbol{\theta}}_I = (1 - \rho) \mathbf{V}_{II}^{-1} \mathbf{V}_I^\top \mathbf{Y} + \rho \mathbf{V}_{II}^{-1} \mathbf{V}_{IJ} \mathbf{V}_{JJ}^{-1} \mathbf{V}_J^\top \mathbf{Y} + \mathbf{H}(\rho),$$

where  $\mathbf{H}(\rho) = \sum_{n=2}^{\infty} \rho^n \mathbf{G}_n$ , for some  $\mathbf{G}_n \in \mathbb{R}^{p_I}$  independent of  $\rho$ . From Lemma A2, we have

$$\begin{aligned} \mathbb{E}(\boldsymbol{\theta}_I^* - \hat{\boldsymbol{\theta}}_I \mid \mathbf{V}_I) \mid_{\rho=0} &= \boldsymbol{\theta}_I^* - \mathbb{E}(\mathbf{V}_{II}^{-1} \mathbf{V}_I^\top \mathbf{Y} \mid \mathbf{V}_I) \\ &= \boldsymbol{\theta}_I^* - \mathbf{V}_{II}^{-1} \mathbf{V}_I^\top \mathbb{E}(\mathbf{Y} \mid \mathbf{V}_I) \\ &= \boldsymbol{\theta}_I^* - \mathbf{V}_{II}^{-1} \mathbf{V}_{II} \boldsymbol{\theta}_I^* = \mathbf{0}. \end{aligned} \quad (\text{A33})$$

It follows that

$$\begin{aligned} \frac{d}{d\rho} B^2(\mathbf{V}_I; \rho) \mid_{\rho=0} \\ = 2 \text{diag}(\tilde{\boldsymbol{\Sigma}}_I)^\top \left[ \mathbb{E}\left\{(\boldsymbol{\theta}_I^* - \hat{\boldsymbol{\theta}}_I) \mid \mathbf{V}_I\right\} \mid_{\rho=0} \circ \frac{d}{d\rho} \mathbb{E}\left\{(\boldsymbol{\theta}_I^* - \hat{\boldsymbol{\theta}}_I) \mid \mathbf{V}_I\right\} \mid_{\rho=0} \right] = 0, \end{aligned} \quad (\text{A34})$$

which implies that an increase of the penalty  $\rho$  around 0 does not effect the bias term. Next we examine the variance term, by law of total variance, we have

$$\begin{aligned} V(\mathbf{V}_I; \rho) &= \text{diag}(\tilde{\boldsymbol{\Sigma}}_I)^\top \text{Var}^\circ(\hat{\boldsymbol{\theta}}_I \mid \mathbf{V}_I) \\ &= \underbrace{\text{diag}(\tilde{\boldsymbol{\Sigma}}_I)^\top \mathbb{E}\left\{\text{Var}^\circ(\hat{\boldsymbol{\theta}}_I \mid \mathbf{V}_I, \mathbf{V}_J) \mid \mathbf{V}_I\right\}}_{V_a(\mathbf{V}_I; \rho)} + \underbrace{\text{diag}(\tilde{\boldsymbol{\Sigma}}_I)^\top \text{Var}^\circ\left\{\mathbb{E}(\hat{\boldsymbol{\theta}}_I \mid \mathbf{V}_I, \mathbf{V}_J) \mid \mathbf{V}_I\right\}}_{V_e(\mathbf{V}_I; \rho)}, \end{aligned} \quad (\text{A35})$$

where the first term is the aleatoric variance and the second term is the epistemic variance.

We first examine the aleatoric variance in (A35). Let

$$\mathbf{M} := (1 - \rho) \mathbf{V}_{II}^{-1} \mathbf{V}_I^\top + \rho \mathbf{V}_{II}^{-1} \mathbf{V}_{IJ} \mathbf{V}_{JJ}^{-1} \mathbf{V}_J^\top + \mathbf{H}_1(\rho),$$

where  $\mathbf{H}_1(\rho) \in \mathbb{R}^{p_I \times n}$  is the higher order term of  $\rho$ . From the from of  $\hat{\boldsymbol{\theta}}_I$  and the conditional distribution of  $\mathbf{Y}$  given  $\mathbf{V}_I, \mathbf{V}_J$ , as characterized in Lemma A1, we have

$$\begin{aligned} \text{Var}^\circ(\hat{\boldsymbol{\theta}}_I \mid \mathbf{V}_I, \mathbf{V}_J) &= \text{Var}^\circ(\mathbf{M} \mathbf{Y} \mid \mathbf{V}_I, \mathbf{V}_J) \\ &= \bar{\sigma}^{*2} \text{diag}(\mathbf{M} \mathbf{M}^\top) \\ &= \bar{\sigma}^{*2} \text{diag}\left(\mathbf{V}_{II}^{-1} + 2\rho(\mathbf{V}_{II}^{-1} \mathbf{V}_{IJ} \mathbf{V}_{JJ}^{-1} \mathbf{V}_{JI} \mathbf{V}_{II}^{-1} - \mathbf{V}_{II}^{-1}) + \mathbf{H}_2(\rho)\right), \end{aligned}$$

where  $\mathbf{H}_2(\rho) \in \mathbb{R}^{p_I \times p_I}$  contains all higher order terms of  $\rho$ . Therefore,

$$\begin{aligned} \frac{d}{d\rho} \text{Var}^\circ(\hat{\boldsymbol{\theta}}_I \mid \mathbf{V}_I, \mathbf{V}_J) \mid_{\rho=0} &= 2\bar{\sigma}^{*2} \text{diag}\left(\mathbf{V}_{II}^{-1} \mathbf{V}_{IJ} \mathbf{V}_{JJ}^{-1} \mathbf{V}_{JI} \mathbf{V}_{II}^{-1} - \mathbf{V}_{II}^{-1}\right) \\ &\quad 2\bar{\sigma}^{*2} \text{diag}\left((\mathbf{V}_{II}^{-1} \mathbf{V}_{IJ} \mathbf{V}_{JJ}^{-1} \mathbf{V}_{JI} - \boldsymbol{\Sigma}_I) \mathbf{V}_{II}^{-1}\right), \end{aligned} \quad (\text{A36})$$

where recall that  $\Sigma_I \in \mathbb{R}^{p_I \times p_I}$  is an identity matrix.

By central limit theorem and Lemma A1, components in (A36) can be approximated as

$$\begin{aligned}\mathbf{V}_{II} &= n\tilde{\Sigma}_I + \mathcal{O}_p(\sqrt{n})\mathbf{1}, \\ \mathbf{V}_{IJ} &= n\mathbf{T}_{IJ} + \mathcal{O}_p(\sqrt{n})\mathbf{1}, \\ \mathbf{V}_{JI} &= n\mathbf{T}_{JI} + \mathcal{O}_p(\sqrt{n})\mathbf{1}, \\ \mathbf{V}_{JJ} &= n\tilde{\Sigma}_J + \mathcal{O}_p(\sqrt{n})\mathbf{1},\end{aligned}\tag{A37}$$

where  $\mathbf{1}$  denotes a matrix with all elements equal to 1, and the notation  $X_n = \mathcal{O}_p(a_n)$  for a sequence of positive constants  $\{a_n\}$  means:  $\forall \epsilon > 0$ ,  $\exists M > 0$  and an integer  $N$  such that  $\mathbb{P}(|X_n/a_n| > M) < \epsilon$ ,  $\forall n > N$ .

Plugging in (A37) into (A36), one can show with some straightforward computation that

$$\mathbf{V}_{II}^{-1}\mathbf{V}_{IJ}\mathbf{V}_{JJ}^{-1}\mathbf{V}_{JI} = \left( \begin{array}{ccc} \sum_{k=1}^{p_J} \frac{(\mathbf{T}_{J:k}^\top \mathbf{T}_{I:1})^2}{(\mathbf{T}_{I:1}^\top \mathbf{T}_{I:1} + \sigma_I^2)(\mathbf{T}_{J:k}^\top \mathbf{T}_{J:k} + \sigma_J^2)} & \cdots & \sum_{k=1}^{p_J} \frac{(\mathbf{T}_{J:k}^\top \mathbf{T}_{I:1})(\mathbf{T}_{J:k}^\top \mathbf{T}_{I:p_I})}{(\mathbf{T}_{I:1}^\top \mathbf{T}_{I:1} + \sigma_I^2)(\mathbf{T}_{J:k}^\top \mathbf{T}_{J:k} + \sigma_J^2)} \\ \sum_{k=1}^{p_J} \frac{(\mathbf{T}_{J:k}^\top \mathbf{T}_{I:2})(\mathbf{T}_{J:k}^\top \mathbf{T}_{I:1})}{(\mathbf{T}_{I:2}^\top \mathbf{T}_{I:2} + \sigma_I^2)(\mathbf{T}_{J:k}^\top \mathbf{T}_{J:k} + \sigma_J^2)} & \cdots & \sum_{k=1}^{p_J} \frac{(\mathbf{T}_{J:k}^\top \mathbf{T}_{I:2})(\mathbf{T}_{J:k}^\top \mathbf{T}_{I:p_I})}{(\mathbf{T}_{I:2}^\top \mathbf{T}_{I:2} + \sigma_I^2)(\mathbf{T}_{J:k}^\top \mathbf{T}_{J:k} + \sigma_J^2)} \\ \vdots & \ddots & \vdots \\ \sum_{k=1}^{p_J} \frac{(\mathbf{T}_{J:k}^\top \mathbf{T}_{I:p_I})(\mathbf{T}_{J:k}^\top \mathbf{T}_{I:1})}{(\mathbf{T}_{I:p_I}^\top \mathbf{T}_{I:p_I} + \sigma_I^2)(\mathbf{T}_{J:k}^\top \mathbf{T}_{J:k} + \sigma_J^2)} & \cdots & \sum_{k=1}^{p_J} \frac{(\mathbf{T}_{J:k}^\top \mathbf{T}_{I:p_I})^2}{(\mathbf{T}_{I:p_I}^\top \mathbf{T}_{I:p_I} + \sigma_I^2)(\mathbf{T}_{J:k}^\top \mathbf{T}_{J:k} + \sigma_J^2)} \end{array} \right) + \mathcal{O}_p(n^{-1/2})\mathbf{1}.$$

Hence,

$$\begin{aligned}\text{diag}\left((\mathbf{V}_{II}^{-1}\mathbf{V}_{IJ}\mathbf{V}_{JJ}^{-1}\mathbf{V}_{JI} - \Sigma_I)\mathbf{V}_{II}^{-1}\right) &= \\ \left( \begin{array}{c} \frac{1}{n(\mathbf{T}_{I:1}^\top \mathbf{T}_{I:1} + \sigma_I^2)} \left( \sum_{k=1}^{p_J} \frac{(\mathbf{T}_{J:k}^\top \mathbf{T}_{I:1})^2}{(\mathbf{T}_{I:1}^\top \mathbf{T}_{I:1} + \sigma_I^2)(\mathbf{T}_{J:k}^\top \mathbf{T}_{J:k} + \sigma_J^2)} - 1 \right) \\ \vdots \\ \frac{1}{n(\mathbf{T}_{I:p_I}^\top \mathbf{T}_{I:p_I} + \sigma_I^2)} \left( \sum_{k=1}^{p_J} \frac{(\mathbf{T}_{J:k}^\top \mathbf{T}_{I:p_I})(\mathbf{T}_{J:k}^\top \mathbf{T}_{I:2})}{(\mathbf{T}_{I:p_I}^\top \mathbf{T}_{I:p_I} + \sigma_I^2)(\mathbf{T}_{J:k}^\top \mathbf{T}_{J:k} + \sigma_J^2)} - 1 \right) \end{array} \right) &+ \mathcal{O}_p(n^{-3/2})\mathbf{1}.\end{aligned}\tag{A38}$$

Putting together (A35), (A36) and (A38), derivative of the aleatoric variance is

$$\begin{aligned}\frac{d}{d\rho} V_a(\mathbf{V}_I; \rho) |_{\rho=0} &= \frac{d}{d\rho} \left[ \text{diag}\left(\tilde{\Sigma}_I\right)^\top \mathbb{E}\left\{\text{Var}^\circ\left(\hat{\theta}_I \mid \mathbf{V}_I, \mathbf{V}_J\right) \mid \mathbf{V}_I\right\} \right] |_{\rho=0} \\ &= \text{diag}\left(\tilde{\Sigma}_I\right)^\top \mathbb{E}\left\{\frac{d}{d\rho} \text{Var}^\circ\left(\hat{\theta}_I \mid \mathbf{V}_I, \mathbf{V}_J\right) |_{\rho=0} \mid \mathbf{V}_I\right\} \\ &= \underbrace{\frac{2\bar{\sigma}^{*2}}{n} \sum_{m=1}^{p_I} \left( \sum_{k=1}^{p_J} \frac{(\mathbf{T}_{J:k}^\top \mathbf{T}_{I:m})^2}{(\mathbf{T}_{I:m}^\top \mathbf{T}_{I:m} + \sigma_I^2)(\mathbf{T}_{J:k}^\top \mathbf{T}_{J:k} + \sigma_J^2)} - 1 \right)}_{:=\Xi} + \mathcal{O}_p(n^{-3/2})\end{aligned}\tag{A39}$$

Let  $\Xi$  denote the asymptotic quantity, from Lemma A4,  $\Xi < 0$ , which implies an increase of penalty  $\rho$  around 0 is beneficial in the sense that it reduces the intrinsic variance of  $\hat{\boldsymbol{\theta}}_I$  given  $\mathbf{V}_I, \mathbf{V}_J$ .

Next, we examine the epistemic variance in (A35), namely,  $\text{diag}(\tilde{\boldsymbol{\Sigma}}_I)^\top \text{Var}^\circ \left\{ \mathbb{E}(\hat{\boldsymbol{\theta}}_I | \mathbf{V}_I, \mathbf{V}_J) | \mathbf{V}_I \right\}$ . Let  $\bar{\boldsymbol{\theta}}_I^*$  be the constant defined in Lemma A1, by definition of conditional variance,

$$\begin{aligned} \text{Var}^\circ \left\{ \mathbb{E}(\hat{\boldsymbol{\theta}}_I | \mathbf{V}_I, \mathbf{V}_J) | \mathbf{V}_I \right\} &= \text{Var}^\circ \left\{ \mathbb{E}(\hat{\boldsymbol{\theta}}_I - \bar{\boldsymbol{\theta}}_I^* | \mathbf{V}_I, \mathbf{V}_J) | \mathbf{V}_I \right\} \\ &= \mathbb{E} \left[ \left\{ \mathbb{E}(\hat{\boldsymbol{\theta}}_I - \bar{\boldsymbol{\theta}}_I^* | \mathbf{V}_I, \mathbf{V}_J) \right\}^{\circ 2} | \mathbf{V}_I \right] - \left[ \mathbb{E} \left\{ \mathbb{E}(\hat{\boldsymbol{\theta}}_I - \bar{\boldsymbol{\theta}}_I^* | \mathbf{V}_I, \mathbf{V}_J) | \mathbf{V}_I \right\} \right]^{\circ 2} \\ &= \mathbb{E} \left[ \left\{ \mathbb{E}(\hat{\boldsymbol{\theta}}_I - \bar{\boldsymbol{\theta}}_I^* | \mathbf{V}_I, \mathbf{V}_J) \right\}^{\circ 2} | \mathbf{V}_I \right] - \left\{ \mathbb{E}(\hat{\boldsymbol{\theta}}_I - \bar{\boldsymbol{\theta}}_I^* | \mathbf{V}_I) \right\}^{\circ 2}. \end{aligned}$$

Therefore,

$$\begin{aligned} &\frac{d}{d\rho} \text{Var}^\circ \left\{ \mathbb{E}(\hat{\boldsymbol{\theta}}_I | \mathbf{V}_I, \mathbf{V}_J) | \mathbf{V}_I \right\} |_{\rho=0} \\ &= \frac{d}{d\rho} \mathbb{E} \left[ \left\{ \mathbb{E}(\hat{\boldsymbol{\theta}}_I - \bar{\boldsymbol{\theta}}_I^* | \mathbf{V}_I, \mathbf{V}_J) \right\}^{\circ 2} | \mathbf{V}_I \right] |_{\rho=0} - \frac{d}{d\rho} \left\{ \mathbb{E}(\hat{\boldsymbol{\theta}}_I - \bar{\boldsymbol{\theta}}_I^* | \mathbf{V}_I) \right\}^{\circ 2} |_{\rho=0}. \end{aligned} \quad (\text{A40})$$

We begin with the first term in (A40), by Leibniz Integral rule,

$$\begin{aligned} &\frac{d}{d\rho} \mathbb{E} \left[ \left\{ \mathbb{E}(\hat{\boldsymbol{\theta}}_I - \bar{\boldsymbol{\theta}}_I^* | \mathbf{V}_I, \mathbf{V}_J) \right\}^{\circ 2} | \mathbf{V}_I \right] |_{\rho=0} \\ &= \mathbb{E} \left[ \frac{d}{d\rho} \left\{ \mathbb{E}(\hat{\boldsymbol{\theta}}_I - \bar{\boldsymbol{\theta}}_I^* | \mathbf{V}_I, \mathbf{V}_J) \right\}^{\circ 2} |_{\rho=0} | \mathbf{V}_I \right] \\ &= 2 \mathbb{E} \left\{ \mathbb{E}(\hat{\boldsymbol{\theta}}_I - \bar{\boldsymbol{\theta}}_I^* | \mathbf{V}_I, \mathbf{V}_J) |_{\rho=0} \circ \frac{d}{d\rho} \mathbb{E}(\hat{\boldsymbol{\theta}}_I - \bar{\boldsymbol{\theta}}_I^* | \mathbf{V}_I, \mathbf{V}_J) |_{\rho=0} | \mathbf{V}_I \right\} \\ &= 2 \mathbb{E} \left\{ \mathbf{V}_{II}^{-1} \mathbf{V}_{IJ} \bar{\boldsymbol{\theta}}_J^* \circ \left( \mathbf{V}_{II}^{-1} \mathbf{V}_{IJ} \mathbf{V}_{JJ}^{-1} \mathbf{V}_{JI} \bar{\boldsymbol{\theta}}_I^* - \bar{\boldsymbol{\theta}}_I^* \right) | \mathbf{V}_I \right\}, \end{aligned} \quad (\text{A41})$$

where the last equality follows directly from Lemma A3.

Next we examine the second term in (A40), by (A33), we have

$$\begin{aligned} &\frac{d}{d\rho} \left\{ \mathbb{E}(\hat{\boldsymbol{\theta}}_I - \bar{\boldsymbol{\theta}}_I^* | \mathbf{V}_I) \right\}^{\circ 2} |_{\rho=0} \\ &= 2 \left\{ \mathbb{E}(\hat{\boldsymbol{\theta}}_I - \bar{\boldsymbol{\theta}}_I^* | \mathbf{V}_I) \right\} |_{\rho=0} \circ \frac{d}{d\rho} \mathbb{E}(\hat{\boldsymbol{\theta}}_I - \bar{\boldsymbol{\theta}}_I^* | \mathbf{V}_I) |_{\rho=0} \\ &= 2(\boldsymbol{\theta}_I^* - \bar{\boldsymbol{\theta}}_I^*) \circ \frac{d}{d\rho} \mathbb{E}(\hat{\boldsymbol{\theta}}_I - \bar{\boldsymbol{\theta}}_I^* | \mathbf{V}_I) |_{\rho=0} \\ &= 2(\boldsymbol{\theta}_I^* - \bar{\boldsymbol{\theta}}_I^*) \circ \mathbb{E} \left\{ \frac{d}{d\rho} \mathbb{E}(\hat{\boldsymbol{\theta}}_I - \bar{\boldsymbol{\theta}}_I^* | \mathbf{V}_I, \mathbf{V}_J) |_{\rho=0} | \mathbf{V}_I \right\} \\ &= 2(\boldsymbol{\theta}_I^* - \bar{\boldsymbol{\theta}}_I^*) \circ \mathbb{E} \left( \mathbf{V}_{II}^{-1} \mathbf{V}_{IJ} \mathbf{V}_{JJ}^{-1} \mathbf{V}_{JI} \bar{\boldsymbol{\theta}}_I^* - \bar{\boldsymbol{\theta}}_I^* | \mathbf{V}_I \right), \end{aligned} \quad (\text{A42})$$

Combining (A37), (A40), (A41) and (A42), we have

$$\begin{aligned}
& \frac{d}{d\rho} V_e(\mathbf{V}_I; \rho) \mid_{\rho=0} \\
&= \frac{d}{d\rho} \text{diag}(\tilde{\Sigma}_I)^\top \text{Var}^\circ \left\{ \mathbb{E}(\hat{\theta}_I \mid \mathbf{V}_I, \mathbf{V}_J) \right\} \mid_{\rho=0} \\
&= 2 \text{diag}(\tilde{\Sigma}_I)^\top \mathbb{E} \left[ \left\{ \mathbf{V}_{II}^{-1} \mathbf{V}_{IJ} \bar{\theta}_J^* - (\theta_I^* - \bar{\theta}_I^*) \right\} \circ \left( \mathbf{V}_{II}^{-1} \mathbf{V}_{IJ} \mathbf{V}_{JJ}^{-1} \mathbf{V}_{JI} \bar{\theta}_I^* - \bar{\theta}_I^* \right) \mid \mathbf{V}_I \right] \\
&= 2 \text{diag}(\tilde{\Sigma}_I)^\top \mathbb{E} \left[ \left\{ \tilde{\Sigma}_I^{-1} \mathbf{T}_{IJ} \bar{\theta}_J^* - (\theta_I^* - \bar{\theta}_I^*) \right\} \circ \left( \tilde{\Sigma}_I^{-1} \mathbf{T}_{IJ} \tilde{\Sigma}_J^{-1} \mathbf{T}_{JI} \bar{\theta}_I^* - \bar{\theta}_I^* \right) \mid \mathbf{V}_I \right] + \mathcal{O}_p(n^{-1/2}) \\
&= 0 + \mathcal{O}_p(n^{-1/2}),
\end{aligned} \tag{A43}$$

where the last equality follows directly from Lemma A5.

In conclusion, from (A32) and (A35), the MSE can be decomposed into

$$\text{MSE}(I; \rho) = B^2(\mathbf{V}_I; \rho) + V_a(\mathbf{V}_I; \rho) + V_e(\mathbf{V}_I; \rho) + \sigma_I^{*2},$$

where by (A34), (A39) and (A43),

$$\begin{aligned}
& \frac{d}{d\rho} B^2(\mathbf{V}_I; \rho) \mid_{\rho=0} = 0, \\
& \frac{d}{d\rho} V_a(\mathbf{V}_I; \rho) \mid_{\rho=0} = \Xi + \mathcal{O}_p(n^{-3/2}), \\
& \frac{d}{d\rho} V_e(\mathbf{V}_I; \rho) \mid_{\rho=0} = 0 + \mathcal{O}_p(n^{-1/2}).
\end{aligned}$$

□

*Proof of Theorem 2.* Let  $\mathbf{v}_I \in \mathbb{R}^{n \times p_I}, \mathbf{v}_J \in \mathbb{R}^{n \times p_J}$  denote the realizations of  $\mathbf{V}_I, \mathbf{V}_J$ . Recall that the definition of  $\mathcal{E}$  is

$$\mathcal{E} = \left\{ \mathbf{v}_I, \mathbf{v}_J \mid \left( \mathbf{v}_{II}^{-1} \mathbf{v}_{IJ} \bar{\theta}_J^* - (\theta_I^* - \bar{\theta}_I^*) \right) \succeq \mathbf{0} \text{ and } \left( \mathbf{v}_{II}^{-1} \mathbf{v}_{IJ} \mathbf{v}_{JJ}^{-1} \mathbf{v}_{JI} \bar{\theta}_I^* - \bar{\theta}_I^* \right) \preceq \mathbf{0} \right\},$$

where the notation  $\mathbf{x} \succeq \mathbf{y}$  (respectively,  $\mathbf{x} \preceq \mathbf{y}$ ) means for  $\mathbf{x}, \mathbf{y} \in \mathbb{R}^d, x_i \geq y_i$  (respectively,  $x_i \leq y_i$ ) for all  $i \in [d]$ .

Next we begin to analyze the bias term under event  $\mathcal{E}$ . From the proof of Theorem 1, we

have that

$$\begin{aligned}
& \frac{d}{d\rho} B^2(\mathbf{V}_I; \rho) \mid_{\rho=0} \\
&= 2\text{diag}\left(\tilde{\Sigma}_I\right)^\top \left[ \mathbb{E}\left\{(\hat{\theta}_I - \theta_I^*) \mid \mathbf{V}_I\right\} \mid_{\rho=0} \circ \frac{d}{d\rho} \mathbb{E}\left\{(\hat{\theta}_I - \theta_I^*) \mid \mathbf{V}_I\right\} \mid_{\rho=0} \right] \\
&= 2\text{diag}\left(\tilde{\Sigma}_I\right)^\top \left[ \mathbb{E}\left\{\mathbb{E}\{(\hat{\theta}_I - \bar{\theta}_I^*) - (\theta_I^* - \bar{\theta}_I^*) \mid \mathbf{V}_I, \mathbf{V}_J\} \mid \mathbf{V}_I\right\} \mid_{\rho=0} \circ \frac{d}{d\rho} \mathbb{E}\left\{(\hat{\theta}_I - \theta_I^*) \mid \mathbf{V}_I\right\} \mid_{\rho=0} \right] \\
&= 2\text{diag}\left(\tilde{\Sigma}_I\right)^\top \left[ \mathbb{E}\left\{\mathbf{V}_{II}^{-1} \mathbf{V}_{IJ} \bar{\theta}_J^* - (\theta_I^* - \bar{\theta}_I^*) \mid \mathbf{V}_I\right\} \circ \frac{d}{d\rho} \mathbb{E}\left\{\mathbb{E}(\hat{\theta}_I - \theta_I^* \mid \mathbf{V}_I, \mathbf{V}_J) \mid \mathbf{V}_I\right\} \mid_{\rho=0} \right] \\
&= 2\text{diag}\left(\tilde{\Sigma}_I\right)^\top \left[ \mathbb{E}\left\{\mathbf{V}_{II}^{-1} \mathbf{V}_{IJ} \bar{\theta}_J^* - (\theta_I^* - \bar{\theta}_I^*) \mid \mathbf{V}_I\right\} \circ \mathbb{E}\left(\mathbf{V}_{II}^{-1} \mathbf{V}_{IJ} \mathbf{V}_{JJ}^{-1} \mathbf{V}_{JI} \bar{\theta}_I^* - \bar{\theta}_I^* \mid \mathbf{V}_I\right) \right] \\
&\leq 0 \text{ under } \mathcal{E},
\end{aligned}$$

where the last equality follows from Lemma A3 and the last inequality follows directly from the definition of  $\mathcal{E}$ . Furthermore, by (A43) in the proof of Theorem 1, derivative of the epistemic variance is

$$\begin{aligned}
\frac{d}{d\rho} V_e(\mathbf{V}_I; \rho) \mid_{\rho=0} &= 2\text{diag}\left(\tilde{\Sigma}_I\right)^\top \mathbb{E}\left[\left\{\mathbf{V}_{II}^{-1} \mathbf{V}_{IJ} \bar{\theta}_J^* - (\theta_I^* - \bar{\theta}_I^*)\right\} \circ \left(\mathbf{V}_{II}^{-1} \mathbf{V}_{IJ} \mathbf{V}_{JJ}^{-1} \mathbf{V}_{JI} \bar{\theta}_I^* - \bar{\theta}_I^*\right) \mid \mathbf{V}_I\right] \\
&\leq 0 \text{ under } \mathcal{E},
\end{aligned}$$

by definition of  $\mathcal{E}$ .  $\square$

*Proof of Corollary 1.* In the special case where  $p = p_I = p_J = 1$ , latent representations  $\mathbf{v}_I, \mathbf{v}_J \in \mathbb{R}^n$  reduces to vectors, the oracle quantities  $T_I, T_J, \bar{\theta}_I^*, \bar{\theta}_J^*$  and  $\theta_I^*$  becomes scalars, and the event  $\mathcal{E}$  in Theorem 2 reduces to

$$\mathcal{E} = \left\{ \mathbf{v}_I, \mathbf{v}_J \mid \frac{\bar{\theta}_J^* \mathbf{v}_I^\top \mathbf{v}_J}{\mathbf{v}_I^\top \mathbf{v}_I} - (\theta_I^* - \bar{\theta}_I^*) \geq 0 \text{ and } \frac{\bar{\theta}_I^* \{(\mathbf{v}_I^\top \mathbf{v}_J)^2 - (\mathbf{v}_J^\top \mathbf{v}_J)(\mathbf{v}_I^\top \mathbf{v}_I)\}}{(\mathbf{v}_J^\top \mathbf{v}_J)(\mathbf{v}_I^\top \mathbf{v}_I)} \leq 0 \right\},$$

Assume without loss of generality that  $T_I, T_J \geq 0$ , from the definition of  $\bar{\theta}_I^*, \bar{\theta}_J^*$  in Lemma A1 and the definition of  $\theta_I^*$  in Lemma A2, we have  $\bar{\theta}_I^*, \bar{\theta}_J^*, \theta_I^* \geq 0$ .

Therefore, the second condition in  $\mathcal{E}$  trivially holds since  $(\mathbf{v}_I^\top \mathbf{v}_J)^2 \leq (\mathbf{v}_J^\top \mathbf{v}_J)(\mathbf{v}_I^\top \mathbf{v}_I)$  for any  $\mathbf{v}_I, \mathbf{v}_J \in \mathbb{R}^n$ . Furthermore

$$\begin{aligned}
\theta_I^* - \bar{\theta}_I^* &= \frac{\theta T_I}{T_I^2 + \sigma_I^2} - \frac{\theta T_I}{\sigma_I^2 + T_I^2 + T_J^2 \sigma_I^2 / \sigma_J^2} \\
&= \frac{\theta T_I (T_J^2 \sigma_I^2 / \sigma_J^2)}{(T_I^2 + \sigma_I^2)(\sigma_I^2 + T_I^2 + T_J^2 \sigma_I^2 / \sigma_J^2)} \\
&= \frac{T_I T_J}{T_I^2 + \sigma_I^2} \cdot \frac{\theta T_J}{\sigma_J^2 + T_J^2 + T_I^2 \sigma_J^2 / \sigma_I^2} = \frac{T_I T_J}{T_I^2 + \sigma_I^2} \bar{\theta}_J^*,
\end{aligned}$$

therefore the first condition in  $\mathcal{E}$  is equivalent as

$$\frac{\mathbf{v}_I^\top \mathbf{v}_J}{\mathbf{v}_I^\top \mathbf{v}_I} \geq \frac{T_I T_J}{T_I^2 + \sigma_I^2}.$$

Hence  $\mathcal{E}$  is equivalent as  $\{\mathbf{v}_I, \mathbf{v}_J \mid \mathbf{v}_I^\top \mathbf{v}_J / \mathbf{v}_I^\top \mathbf{v}_I \geq T_I T_J / (T_I^2 + \sigma_I^2)\}$ .  $\square$

## A5 Supplementary Tables and Figures

Here, we present additional results that extend those shown in the main manuscript. Tables A3 to A7 show that our proposed Meta Fusion strategy outperforms alternative ensemble techniques. Figure A7 provides detailed results for the neural decoding task.

	Setting 1.1	Setting 1.2	Setting 1.3
Best Single (ind.)	5.51 (0.09)	43.86 (0.69)	53.94 (0.88)
Best Single	5.33 (0.09)	42.13 (0.68)	53.61 (0.90)
Meta Fusion	<b>5.07 (0.08)</b>	<b>38.51 (0.64)</b>	<b>49.59 (0.84)</b>
Stacking	5.20 (0.08)	<b>38.73 (0.67)</b>	52.99 (0.90)
Simple Avg.	10.87 (0.17)	59.57 (0.94)	73.04 (1.18)
Weighted Avg.	5.29 (0.09)	42.72 (0.73)	58.16 (0.98)

Table A3: Comparison of various ensemble techniques under the settings described in Section 5.1. The details are the same as in Table 1.

	Setting 2.1	Setting 2.2	Setting 2.3
Best Single (ind.)	2.70 (0.06)	60.20 (1.53)	60.14 (1.53)
Best Single	2.63 (0.06)	57.61 (1.51)	57.30 (1.49)
Meta Fusion	<b>2.47 (0.06)</b>	<b>52.27 (1.35)</b>	<b>53.38 (1.40)</b>
Stacking	<b>2.51 (0.06)</b>	61.11 (1.95)	64.51 (1.72)
Simple Avg.	<b>2.48 (0.06)</b>	60.72 (1.57)	64.99 (1.66)
Weighted Avg.	<b>2.47 (0.06)</b>	59.80 (1.55)	63.47 (1.62)

Table A4: Comparison of various ensemble techniques under the settings described in Section 5.2. The details are the same as in Table 2.

	Mean Acc (SE)
Best Single (ind.)	0.7944 (0.0020)
Best Single	0.7980 (0.0020)
Meta Fusion	<b>0.8004 (0.0019)</b>
Stacking	0.7272 (0.0050)
Simple Avg.	0.7966 (0.0021)
Weighted Avg.	0.7968 (0.0021)
Majority Vote	0.7961 (0.0020)
Weighted Vote	0.7961 (0.0020)

Table A5: Classification accuracies and the corresponding standard errors for Alzheimer’s disease detection (Section 6.1) using various ensemble techniques.

	Barat	Buchanan	Mitt	Stella	Superchris
Best Single (ind.)	0.556 (0.010)	0.768 (0.007)	0.619 (0.008)	0.632 (0.007)	<b>0.768 (0.008)</b>
Best Single	0.608 (0.010)	0.780 (0.009)	<b>0.630 (0.008)</b>	0.649 (0.010)	<b>0.766 (0.009)</b>
Meta Fusion	<b>0.625 (0.010)</b>	<b>0.787 (0.007)</b>	<b>0.622 (0.008)</b>	<b>0.677 (0.011)</b>	<b>0.767 (0.009)</b>
Stacking	0.562 (0.012)	0.693 (0.010)	0.495 (0.012)	0.591 (0.011)	0.660 (0.013)
Simple Avg.	<b>0.621 (0.010)</b>	0.774 (0.008)	0.560 (0.009)	0.644 (0.009)	0.704 (0.009)
Weighted Avg.	<b>0.622 (0.010)</b>	<b>0.789 (0.007)</b>	0.579 (0.008)	0.648 (0.009)	0.738 (0.008)
Majority Vote	0.601 (0.010)	0.751 (0.008)	0.414 (0.008)	0.618 (0.010)	0.510 (0.009)
Weighted Vote	<b>0.618 (0.010)</b>	<b>0.786 (0.007)</b>	0.462 (0.008)	0.628 (0.010)	0.689 (0.010)

Table A6: Ensemble Technique Comparison

Table A7: Classification accuracies and the corresponding standard errors for neural decoding (Section 6.2) across five rats using various ensemble techniques. Bold numbers indicate mean accuracy within 1 SE of the highest value across all methods.

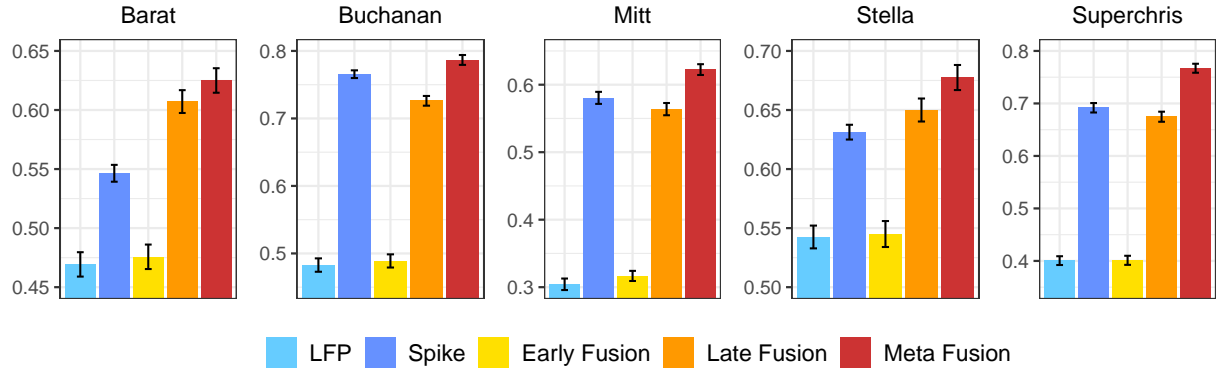


Figure A7: Classification accuracies for neural decoding across five rats using various data fusion strategies (see Section 6.2; these are extended results for Figure 4). Error bars indicate standard errors.